P-65

NASA Contractor Report 189677

Evaluation of a Doubly-Swept Blade Tip for Rotorcraft Noise Reduction

Brian E. Wake and T. Alan Egolf
United Technologies Research Center
East Hartford, CT

Contract NAS1-19143
October 1992

NOTICE

National Aeronautics and Space Administration

Langley Research Center
Hampton, Virginia 23665-5225

Review for general release (2 years from date of publication).

NASA Contractor Report 189677

Evaluation of a Doubly-Swept Blade Tip for Rotorcraft Noise Reduction

Brian E. Wake and T. Alan Egolf
United Technologies Research Center
East Hartford, CT

Contract NAS1-19143
October 1992

NOTICE

National Aeronautics and
Space Administration

Langley Research Center
Hampton, Virginia 23665-5225

PREFACE

The work reported herein was conducted under contract NAS1-19143, Advanced Concepts for Civil Rotorcraft Noise Reduction, National Aeronautics and Space Administration, Langley Research Center. The work was initiated on 20 November 1990 and completed 15 October 1992.

The Government Technical Representative for this contract was Earl Booth of NASA Langley Research Center. The principal investigator was T. Alan Egolf, Senior Principal Engineer, the co-investigator was Brian E. Wake, Research Engineer, and the program manager was Anton J. Landgrebe, Manager, Aeromechanics Research. Joe Visintainer of Sikorsky Aircraft performed the acoustic calculations. The NAS computer facilities at NASA Ames Research Center were used for the Navier-Stokes calculations.

TABLE OF CONTENTS

SUMMARY

A computational study was performed for a doubly-swept rotor blade-tip design concept to determine its merit to reduce high-speed impulsive (HSI) noise and blade-vortex interaction (BVI) noise. The tip design employs both aft sweep and forward sweep.

For the HSI-noise computations, unsteady Euler calculations were performed for several variations of a rotor-blade geometry. These variations were based on UH-60A Black Hawk rotor-blade twist, chord, and airfoil section type using the original doubly-swept tip planform originally developed by M. Tauber at NASA Ames. The goal of this study was to use the doubly-swept planforms and develop a new blade-tip design that would reduce BVI noise while retaining the HSI benefits of the NASA design. The original doubly-swept planform, studied in earlier NASA investigations, was found to have the highest delocalizing Mach number (0.95) and thus the potentially lowest HSI noise, but it has an effective *forward* sweep on a thrust-weighted basis. For aeroelastic considerations, a doubly-swept planform with a thrust-weighted effective *aft* sweep was developed which has a delocalizing Mach number of 0.94. This blade planform was used as a starting point in the BVI-noise study. Along with the successful definition of a lower HSI-noise rotor than the baseline Black Hawk rotor, other studies included comparisons between quasi-steady and unsteady results, and Euler versus Navier-Stokes results.

For the BVI-noise problem, it had been hypothesized that the doubly-swept blade tip, by producing a leading-edge vortex, would affect the downstream vorticity distribution in a manner which would reduce the tip-vortex effect in BVI noise. In the present work, the velocity profiles downstream of the helicopter blades as computed by a Navier-Stokes solver were used along with auxiliary codes to produce a model of the inflow of a BVI event. This inflow distribution was then used by an unsteady Euler analysis to predict the pressure distributions associated with this BVI event. An acoustic analysis, WOPWOP, used these pressure distributions to compute the resultant noise. This study was inconclusive, in part, because the Navier-Stokes calculations did to resolve the vortex roll-up process accurately. As a result, acoustic calculations for the baseline UH-60A case did not compare well with experimental acoustic results. The problem with the Navier-Stokes calculations has been identified as vorticity dissipation. This may be due to insufficient grid resolution as limited by the computer resource constraints of this investigation. In addition, due to the low loading at the tip for the advancing side and operating condition studied, there was no indication of a leading-edge vortex formation.

The doubly-swept blade offers a potential benefit for HSI-noise reduction over the aft-swept Black Hawk blade, but experimental studies or improved high-resolution calculations are needed to determine the potential, if any, of the doubly-swept blade for BVI-noise reduction.

LIST OF SYMBOLS

a_∞	freestream speed-of-sound
c	blade chord
C_n	sectional normal force coefficient of blade
C_t	sectional thrust coefficient of blade
C_L	lift coefficient of rotor, $C_L = L/\rho_\infty \pi R^2 (\Omega R)^2$
L	lift of rotor
M_{adv}	advancing tip Mach number, $M_{adv} = M_{hov}(1+\mu)$
$M_{delocal}$	delocalizing Mach number
M_{hov}	rotational tip Mach number, $M_{hov} = \Omega R/a_\infty$
r	distance from the rotor hub
R	rotor radius
t	blade thickness
V	magnitude of velocity
V_∞	flight velocity
w	axial velocity
y	spanwise coordinate along the blade
ρ_∞	freestream fluid density
ψ	azimuth coordinate
Ω	rotor rotational speed
μ	advance ratio, $\mu = V_\infty/\Omega R$
σ	solidity of the rotor
α_{tpp}	tilt of the tip path plane, positive for nose-up tilt.
α_{twist}	rotor-blade twist
ϕ	longitudinal angle from rotor hub
θ	lateral angle from rotor hub

INTRODUCTION

In order to successfully reduce rotor noise, it is necessary to attack the problem at the fundamental level of the noise-producing mechanisms. High-speed impulsive (HSI) noise mechanisms associated with compressibility have been found to be fundamentally dependent on blade-tip aerodynamics, while blade-vortex interaction (BVI) noise is dependent on the tip-vortex structure which is affected by the tip aerodynamics. In previous exploratory studies of noise mechanisms at NASA and the United Technologies Research Center (UTRC) using first-order modeling assumptions, predicted influences of forward tip sweep on the tip pressure field and wake have indicated a potential acoustic benefit. Specifically, the potential of delaying sonic delocalization associated with high-speed impulsive noise and redistributing tip vorticity for reduced BVI noise has been identified, and studies with more rigorous aerodynamic modeling and acoustic prediction were recommended.

In this computational study, aerodynamic mechanisms are modeled to reduce high-speed impulsive noise and blade-vortex interaction noise. Both of these impulsive noise mechanisms are addressed using advanced blade tips with doubly-swept planforms, the baseline doubly-swept planform developed in Refs. 1 and 2 and a modified doubly-swept planform (Figure 1). The doubly-swept planforms consists of forward sweep at the tip and aft sweep inboard of the forward sweep. For this study, state-of-the-art rotor airloads, airflow, and noise-prediction codes are used to investigate the potential of such a design concept for the reduction of rotorcraft noise. The assessment of noise reduction was made by comparing predicted magnitudes of acoustic information for an existing rotor-blade design (Black Hawk, UH-60A, also shown in Figure 1) and the doubly-swept tip designs. Since the study relies on several modeling assumptions, it is considered to be a conceptual study.

Background

Rotor blades of conventional rotorcraft operate in a general unsteady compressible aerodynamic environment which is also subject to very localized blade-vortex interactions. Both the unsteady compressible aspects of the flow and the BVI events are sources of impulsive noise unique to rotorcraft. High-speed impulsive noise is associated with compressibility on the advancing side of the rotor disk due to the occurrence of regions of supersonic flow on the blade. This source of noise can occur independent of blade loading (Ref. 3), and is a function of blade-thickness distribution, planform geometry, and flight condition. Generally, the impulsive noise associated with blade-vortex interaction events are associated with low-speed flight and descent conditions, although BVI can occur over a wide spectrum of flight conditions, depending on rotor speed, attitude, and loading conditions. For the general low-speed and descent conditions, noise associated with a BVI event is caused by local unsteady blade loading on the aft region of the rotor disk (but not restricted to this region). Relatively large and rapid changes in the local induced velocity

field associated with the close passage of tip vortices nearly parallel to the blade cause unsteady blade loading.

Modeling of these impulsive noise mechanisms is not yet at the level of sophistication required to consistently predict the correct acoustic signature. However, progress is being made in the acoustic side of the prediction area. For example, in Ref. 4, using actual experimental blade-surface pressure distributions and some approximations to define the non-linear quadrupole strengths, good acoustic predictions for both compressibility (Figure 2) and BVI impulsive noise (Figure 3) have been obtained. The results of Ref. 5-7 also show acceptable BVI impulsive noise predictions using experimental surface pressures. Thus, it would appear that the major problem in producing good acoustic predictions is in the prediction of the blade airloading. In Ref. 8, two different aerodynamic/aeroacoustic methodologies are used to make acoustic predictions for a helicopter rotor. Both methodologies use linear acoustic methods and a prescribed vortex-lattice wake model to obtain the wake-induced inflow. The best results were obtained with the ROTONET method (Refs. 9 and 10) which used the more detailed wake model, a generalized distorted forward-flight wake (Refs. 11 and 12). However, the predictions from both methods were still significantly less accurate than predictions shown in Refs. 4-7 using measured airloads. Both linear methods, used in Ref. 8, rely on fundamentally two-dimensional aerodynamic models based on strip theory and thus neglect three-dimensional effects in the blade airloadings. In addition, there is some concern that the lack of a non-linear noise model and the temporal resolution of the load-prediction methodologies affects the quality of the acoustic prediction. From these sample references, it is apparent that the accuracy of the acoustic predictions is very dependent on the ability to predict the blade-surface pressures and possibly the off-blade values (quadrupole source terms).

The prediction of BVI impulsive noise is strongly dependent on the ability to model both the rotor wake, and blade-loading response associated with the event. If either of the models is deficient, the corresponding prediction would be questionable. Recent work (Ref. 13) has demonstrated that present freewake methods do a fairly good job in predicting the locations of BVI events. But these models lack a consistent accuracy over the entire rotor disc, especially for difficult flight conditions, such as descent, where BVI occurs. The use of more sophisticated unsteady three-dimensional flow codes and wake models is starting to address the loading response issue, but much more remains to be done to improve the wake-modeling aspect of the problem.

There has been recent work in the area of improving forward-flight wake models, where researchers are attempting to model the complete wake surface as a distorting surface as exemplified in Refs. 14-17. Earlier wake models have used built-in simplifying assumptions regarding the structure of the wake to reduce computational cost. In particular, the assumption of a single tip-vortex structure, and a non-distorting inboard sheet are common models upon which early free-wake methods are based. For certain types of rotor-blade designs and flight conditions, these built-in assumptions have proved to be incorrect (Refs. 14 and 15). Faster computers are making the reliance on these simplifying assumptions unnecessary (Ref. 17).

The incorporation of the effect of the wake into advanced finite-difference and finite-volume three-dimensional rotor-blade flow solvers has also been advancing. These methods have the advantage of being able to predict the non-linear flow characteristics both on and off the rotor blade, but computational cost is still a major concern for the viscous analyses. In addition, the incorporation of the wake influence is more difficult than with earlier lifting-line, lifting-surface, and panel methods (traditionally linear models) due to numerical and CPU cost considerations. However, in recognition of the need to include the wake influence for accurate predictions, the modeling of the wake effects has progressed from simple angle-of-attack adjustments to the more sophisticated wake-embedding techniques using complex three-dimensional wake geometries. Most of the work in this area has been focused on the potential formulations (Refs. 18-24) because of the inherently higher computational cost associated with Euler and Navier-Stokes solvers. Researchers have been progressively improving the prediction methods from transonic small-disturbance methods (Ref. 20) to full-potential methods with a variety of wake-modeling approaches (Refs. 21-23,25). A sophisticated full-potential/wake method incorporates the convection of the wake internal to the solution process (Ref. 23), but is currently limited to hover. There has been work done by researchers on wake modeling in Euler and Navier-Stokes solvers (e.g. Refs. 26-30), but the degree of sophistication of the wake models is not as advanced as for the potential formulations. Generally, the wake effect is modeled as an inflow adjustment at the blade. The embedded-wake methodology, for hover applications, was incorporated into the Euler mode of the first rotor-blade viscous flow solver, NSR3D (Ref. 31-33). Recent work with a less-dissipative up-winded scheme (Ref. 34) and an adaptive-grid method (Ref. 35) have attempted to compute the tip vortex for several rotor revolutions. Results to date are promising. Most of the net downwash appears to be captured, but accurate resolution of the tip-vortex velocity profiles is lost due to numerical diffusion. More validation and grid studies are required for these methods. Again, although generally too expensive for detailed design work today, new computer architectures will resolve the computational cost issue for these viscous code applications (Ref. 32) in the near future.

Design Concept

The advanced blade-design concept investigated in this study is a doubly-swept blade, aft-swept inboard of the blade tip and then forward-swept to the blade tip, to reduce both the compressibility and BVI related noise. A doubly-swept design, originally developed by M. Tauber of the NASA Ames Research Center (Ref. 2) and shown in Figure 1, was used as the initial input to this study. The justification to study such a concept has evolved from insight into past numerical and empirical studies. There are two primary reasons to consider forward-swept blade designs, one associated with each HSI noise and BVI noise. The first, and generally accepted reason, is to reduce the effective Mach number at the blade tip. It is well known that aft-swept blades delay the occurrence of the strongest compressibility effects on the advancing side of the rotor disk. On the basis of geometric considerations and accepted two-dimensional swept-flow theory, the delay in rotor azimuth is equal to the blade sweep angle, neglecting any change in the relative velocity.

In an ideal two-dimensional sense, the benefit would be identical for both aft- and forward-swept blades. However, additional three-dimensional effects enter into the picture. Numerical predictions are presented in Ref. 1 for straight, aft-swept, and forward-swept blade designs using the full-potential method of Ref. 25. This study demonstrated the acoustic benefits of the forward-swept blade compared with the straight and aft-swept blades, at selected azimuthal positions. In Figure 4, Mach contours are shown from Ref. 1 for aft-swept and forward-swept blade-tip designs at ψ = 90 degrees, for μ = 0.41 and M_{hov}=0.65, which gives an advancing tip Mach number of 0.92. The predicted results, based on inviscid, quasi-steady full-potential theory, indicated that the forward-swept blade was superior to the conventional aft-swept blade for reducing the extent of delocalization and for reducing the inviscid torque.

The delocalization concept is based on the premise that if there exists a region of supersonic flow, relative to the blade, that extends to the sonic surface (or sonic cylinder) off the blade, then efficient propagation of acoustic energy occurs. The sonic surface is the iso-Mach surface of Mach number equal to 1.0 in the hub-centered, blade-fixed coordinate system. Thus, if the supersonic region does not extend to the sonic surface off the blade, then the acoustic signature is weaker. The results shown in Ref. 36 seem to confirm the use of delocalization as an acceptable indication of acoustic signal strength associated with the transonic non-linear effects. In Figure 4, sonic delocalization is present for the aft-swept design.

The forward-swept blade designs studied in Ref. 1 may produce destabilizing aeroelastic effects. The purely forward-swept blade tip moves the effective blade-tip aerodynamic center forward of the blade elastic axis. This can result in torsional deflections which tend to increase with increasing loading, resulting in even higher tip loads, unlike straight and aft-swept blade tip designs. Follow-up work presented in Ref. 2 by Tauber addressed this issue in conjunction with numerical optimization techniques applied to the full-potential flow analysis for minimizing the delocalization region for a doubly-swept blade tip. In this study, the inboard portion of the blade tip was swept aft in the conventional manner, while the outermost section was swept forward. The inboard aft sweep balances the negative aeroelastic effects of the outboard forward sweep. Only selected azimuthal positions were studied, but the doubly-swept design, including tailored airfoil sections was able to produce significantly reduced delocalization regions (i.e. reduced acoustic signal strength) with reduced inviscid torque and acceptable blade-pitching moments. A subsequent change in the sweep was able to remove the delocalization without tailored airfoil sections. One of the purposes of the present study is to validate these earlier calculations which relied on quasi-steady full-potential methods. This study addresses the effect of entropy changes (Euler equations), unsteadiness, and viscosity on the prediction of delocalization for this concept.

A second reason to sweep the blade tip forward is to affect the tip-vortex structure to reduce the BVI noise. Recent experimental work, Ref. 37, has demonstrated that forward-swept wing geometries reduce the amplitude of the velocity field associated with the vortex-flow structure produced by unsteady oscillating wings. This experimental program

was focused on unsteady, oscillating wings with different swept planforms. Although these results do not truly reflect the aerodynamic environment of the rotor blade they are indicative of the potential of changing the downstream velocity field associated with the different planforms. In Figure 5, taken from Ref. 37, velocity profiles for forward-swept, straight, and aft-swept wings are shown as a function of one period of oscillation of the wing at a point 0.17 chord lengths (0.17c) downstream of the wing-tip leading edge and 0.10 chords above the blade surface. Comparison of the peak-to-peak values in the velocity profiles indicate that the value of the forward-swept wing is half of the aft-swept wing value. Additional results comparing the same information and wing geometries at four different spanwise positions demonstrated a consistently weaker velocity field than the aft-swept and straight wing.

Additional experimental results, Refs. 38 and 39, for aft-swept, straight, and forward-swept vanes has shown that the wake of the forward-swept vane produced the least noise when ingested into a rotating blade system. Flow measurements at UTRC indicated that the velocity field downstream of the forward-swept vane was weaker than the others, similar to the results for the wing of Ref. 37. It was hypothesized that the vorticity of a leading-edge vortex is entrained into the tip-vortex structure for the aft-swept vane, increasing the magnitude of the velocity components. Conversely, for the forward-swept vane, it is hypothesized that the vorticity of a leading-edge vortex stays separate from the tip vortex, and eventually leaves the blade inboard of the traditional tip-vortex location of the straight and aft-swept vane. The result is that the vorticity is more distributed and the tip vortex is therefore weaker. This weaker velocity field is the reason for the weaker acoustic signal. These different sets of experimental data support the idea that the flow structure of a forward-swept rotor-blade tip may produce a significantly weaker flow structure than an aft-swept or straight blade tip.

Some preliminary unpublished predictions of the forward- and aft-swept vanes were made using the NSR3D code described in Refs. 31-33. The calculations demonstrated the differences in leading-edge vortex and tip-vortex formations for the two configurations. The differences in flow structure, i.e. the convection of the leading-edge vortex, were also computed for the rotating flow field of aft-swept and forward-swept prop-fans. On this basis, the design concept study was initiated.

TECHNICAL APPROACH

The purpose of this study is to refine an initial doubly-swept design planform from Ref. 2 to have good high-speed impulsive noise (HSI) characteristics and produce a weakened tip-vortex structure to reduce its blade-vortex interaction (BVI) noise. This required two major prediction activities. The first major activity was the application of an unsteady Euler method to validate earlier quasi-steady full-potential findings for this concept and refine the doubly-swept geometry to provide an effective aft-sweep while maintaining its HSI-noise benefit over the Black Hawk rotor. The second major activity involved the use of a Navier-Stokes code to define the flow structure downstream of the doubly-swept rotor-blade tip. This information was used to define a BVI-wake-induced velocity for use in the Euler analysis to study the effect of the tip shape on blade-vortex interaction related noise. These predictions included the following computer codes, a modified vortex-lattice method (BVI_INFLOW), the UTRC three-dimensional Navier-Stokes/Euler rotor analysis (NSR3D), and the government-funded acoustic prediction code (WOPWOP). Each of these analyses, and their coupling, will be described in this section.

High-Speed Impulsive Noise Methodology

To rigorously predict the compressibility noise, the non-linear flow field must be calculated. This precludes the use of traditional linear methods, such as lifting-surface or panel methods. A flow solver with transonic capability is required to predict the region of supersonic flow associated with the delocalization and the three-dimensional pressure field. The ability to predict the acoustic far-field using finite-difference (or finite-volume) methods has been successful in two-dimensions and is very costly. The equivalent three-dimensional calculation is currently computationally prohibitive. Work is progressing in the area of combining these finite-difference methods for the accurate near-field calculation of the non-linear effects with linear methods for the far-field. The most notable successes have been limited to modeling two-dimensional impulsive events to investigating the three-dimensional propagation of the signal (Refs. 40 and 41), and hover applications (Refs. 42 and 43) using the FPR code of Ref. 21. Both of these approaches used a Kirchhoff formula for the linear far-field model. A study of recent literature indicates that the extension of this approach to forward flight has not been demonstrated. However, the non-linear near-field solution can be used as an indicator of the acoustic strength using the concept of delocalization. This is the approach that is used in this HSI-noise reduction study.

For a given geometry, the critical parameter governing the existence of delocalization is the advancing tip Mach number (M_{adv}). This is the Mach number the blade tip experiences on the advancing side of the rotor. As M_{adv} is increased (whether through increase of forward-flight speed or rotational speed), the supersonic region gets larger and the sonic surface moves closer to the blade. Eventually, an advancing tip Mach number is reached at which the supersonic region intersects with the sonic surface. This limiting M_{adv} is referred to as the "delocalizing Mach number", and is denoted as $M_{delocal}$. To determine the delocalizing Mach number for various geometries, unsteady Euler calculations

were performed using NSR3D (described below) in the Euler mode. Today's conventional rotorcraft are limited to a maximum advance ratio of approximately 0.46 due to the onset of dynamic stall. This limit is independent of the transonic acoustics. For these runs, the advance ratio was fixed to this estimate of the maximum advance ratio. By increasing the rotational speed of the rotor at this maximum advance ratio, the forward-flight speed of the helicopter is maximized. For various geometries the rotational tip Mach number was increased until delocalization was predicted by the unsteady Euler solver. A Glauret linear inflow model was used, where the inflow varies linearly with radius at a given azimuth location. The parameters for this model can be derived from classical vortex theory. The effect of blade loading, and hence the wake, at these high speeds on delocalization is secondary (Ref. 3), thus this linear inflow model is assumed adequate for relative comparison between geometries.

Blade-Vortex Interaction Noise Methodology

The modeling of BVI-related phenomena is completely dependent on the wake-geometry model; in particular, the distortion of the wake geometry and hence the wake-vorticity distribution. In addition, the prediction of unsteady wake/blade interaction is difficult because the blade may modify or destroy the vortex during the interaction. Recent efforts are starting to address BVI modeling in three dimensional Euler and Navier-Stokes solvers using prescribed wake geometries (Ref. 30), but the complete rigorous prediction is beyond the capability of current analyses.

For the present study, a coupled methodology is used to model the BVI event. A flow chart of the coupled methodology process for BVI-noise prediction is given in Figure 6. The first step of the process is to determine the azimuthal positions of the BVI events for a given flight condition. This can be performed using the wake geometry charts of Ref. 44 and referring to experimental data (Refs. 45-47). For the purpose of this investigation, the effort focuses on the BVI events in the first quadrant of the rotor disk. Once the BVI event is identified, the wake age of the interacting wake element can be approximately determined using the charts of Ref. 44, and thus the blade azimuth position at which the tip-vortex structure is generated can be determined. This is the azimuthal position at which the viscous flow solver (NSR3D) is run in the quasi-steady mode to estimate the flow structure of the trailing tip-vortex structure of the blade-tip design.

Once the viscous flow field near the blade at the designated azimuth location is computed, the axial velocity component downstream of the blade must be extracted and incorporated into the vortex-lattice wake method. Here, the axial direction is defined as perpendicular to the rotor-shaft plane, this is the direction which will have the largest effect on blade loads. The modified vortex-lattice method, called BVI_INFLOW, uses the computed input axial velocity distribution to predict the induced inflow for specific BVI events. The prediction process uses this input axial velocity profile in place of the Biot-Savart law for the axial induced-flow behavior. Only vortex segments which have a significant impact on the BVI event are included in the calculation. The interaction is

very sensitive to the distance between the vortex and the blade. Since this distance cannot be computed accurately, the wake is given zero axial displacement. This simplification produces the maximum BVI effect and eliminates uncertainties in the prediction of the wake geometry. The tip vortex is assumed to impact the blade without disrupting the vortex. The mapping of this input velocity profile to a vortex-segment-induced value is based on the orthogonal distance from the vortex segment to the point being influenced. A decay behavior which is inversely proportional to distance, similar to Biot-Savart, is used beyond the range of the input profile. The BVI induced effects at the interacting blade are calculated over a specified azimuthal region. This data is then linearly faired to zero at the blade root and linearly interpolated azimuthally from the edges of the specified region over the remaining azimuthal region to produce a smooth inflow variation away from the BVI event.

This BVI-inflow-modeling process makes two assumptions which must be recognized. The first assumption is that the tip-wake structure aft of the blade trailing edge is maintained as the tip wake is convected in space and time to the blade undergoing the BVI event. Currently this viscous phenomena cannot be accurately predicted very far downstream of the blade with any current analysis code, due to the combination of extreme cost and numerical dissipation. The second assumption is that the quasi-steady viscous-flow prediction of the flow structure is adequate to define the relative differences in the wake and flow structure between different blade-tip designs.

The inflow distribution over the entire rotor disc is then provided to the unsteady Euler solver. The Euler solver is used to compute the blade surface pressure distribution for a complete rotor revolution. These pressures are provided to the acoustics analysis to predict the corresponding noise.

Navier-Stokes/Euler Solver

The unsteady Euler calculations and the viscous calculations for the tip-vortex velocity profiles were obtained using the Euler/Navier-Stokes analysis (NSR3D). This Navier-Stokes analysis (NSR3D), originally developed by Wake and Sankar (Ref. 31), has since been significantly refined at UTRC (Refs. 32 and 33).

The numerical procedure, which is a modification of the Beam and Warming algorithm (Refs. 48 and 49), has unsteady capability and does not make the thin-layer assumption. The spanwise-flux terms are treated explicitly in time. Lagging the spanwise terms gives a hybrid procedure which performs implicit inversions in the airfoil planes, but marches explicitly in the spanwise direction. It was shown in Ref. 50 that such a hybrid procedure works well when the spacing in the spanwise direction is much larger than in the other two. The viscous terms are treated explicitly in time as well. It has been demonstrated by others that evaluating the viscous terms explicitly is stable for high Reynolds number flows (above 100,000, typical for this study) provided adequate implicit dissipation is employed (Refs. 51 and 52). In the present analysis, the viscous terms are approximately treated in the diagonalized form of the left-hand side (Ref. 53)

To enhance convergence and produce accurate unsteady results, a Newton sub-iteration scheme with local time stepping is utilized within each global time step (Ref. 54). To maintain time accuracy, the unsteady term is included in the residual on the right-hand side of the equations. The sub-iterations reduce the errors in the left-hand side associated with approximate factorization, diagonalization, and explicit treatment of the viscous terms and boundary conditions. The result of using this scheme is an essentially fully implicit algorithm. By using three or four sub-iterations with local time-stepping, it has been found that the time step can be increased by a factor of ten or more for these problems. The benefits are primarily for unsteady problems but convergence is improved for steady problems as well.

The code can use a variety of grid types, but the C-grid is generally preferred and was used in this study. In NSR3D, a sheared parabolic C-grid is algebraically generated internal to the code. Two views of the grid at a given spanwise station for Euler calculations is provided in Figures 7a and 7b. For the Navier-Stokes calculations a much finer mesh is used in the normal direction.

The use of standard central differences to approximate spatial derivatives can give rise to odd-even decoupling and cascading high-frequency errors. To control these problems, blended 2nd/4th-order artificial dissipation terms are added explicitly to the right-hand side of the equations as described by Jameson (Ref. 55). Fourth-order implicit dissipation is added to the left-hand side to improve the overall stability of the algorithm. This leads to a pentadiagonal system of equations which can be solved efficiently when using the diagonalized form of the equations.

A modification of the well-known Baldwin-Lomax algebraic turbulence model is used (Ref. 56). This model is adequate for attached or mildly separated flows but is not reliable in massively separated regions. This model, however, has proven to do nearly as well as the much more costly one- or two-equation models and presently the advantages of the higher-order models are not evident in all applications (Ref. 57). In the original Baldwin-Lomax model (Ref. 56), calculation of the normal distance from the wall for the inner layer uses shear values at the wall. For the modified version, the maximum normal shear value is used (Ref. 58) instead of the wall shear stress because in the vicinity of separation points, the wall shear stress will approach zero. For computing the maximum of the wake function in the model, the search is limited in the normal direction. This modification, similar to that of Ref. 59 for slender bodies, improves the model where cross-flow separation is present. An exponential blending function is incorporated to smooth the transition between the inner and outer eddy-viscosity distributions.

An unsteady grid is employed to account for the motion of the rotor blade. Any motion of the blade due to cyclic pitch or flapping is included in the unsteady grid-motion terms. Lead-lag motion could also be included in these terms, but its effect on the aerodynamic loading is small. Using these unsteady terms, large and arbitrary blade motions can be accounted for in an accurate and very convenient manner.

For simplicity, and to give a flexible solution procedure, all boundary conditions are applied explicitly. That is, after the interior points have been solved for, the values at the boundaries are updated. Implicit treatment of the boundaries enable slightly larger time steps, but produces a very inflexible scheme since the boundary conditions must be built into the inversion process.

At the surface of the blade, the no-slip conditions are applied for viscous solutions, while tangency is applied for inviscid solutions. For density and pressure at the blade surface, their normal derivatives are specified to be zero. This is equivalent to an adiabatic wall condition. At the far-field boundaries, quantities are either fixed or extrapolated depending on whether the flow is inflow or outflow and subsonic or supersonic. For supersonic inflow, all quantities are set to freestream values, for subsonic inflow, the density is extrapolated to allow for the propagation of one characteristic. At the outflow boundaries, all quantities are extrapolated except for pressure which is set to freestream. Extrapolating pressure, even for supersonic outflow, tends to be destabilizing.

At the most inboard spanwise station, one-sided differencing is used in the spanwise direction for the convective terms, while the spanwise viscous terms are turned off. At the cut surface formed by the C-grid, quantities are averaged from above and below.

The Navier-Stokes/Euler solver (NSR3D) is dependent upon a very simple method for the inclusion of the wake effects. The wake velocities are included in the surface boundary conditions. These velocities have a radial and chordwise variation over the blade surface.

Acoustics

The impulsive noise due to the BVI events was predicted by using the NASA acoustic prediction code, commonly called WOPWOP (Ref. 60). This analysis uses the linear model on which the ROTONET program is based, but is easier to run in a stand-alone mode. This feature is very desirable because the main focus of the investigation is to address only the compressibility and BVI loading noise on a relative basis.

The analysis utilizes numerical analysis techniques applied to Farassat's solution of the Ffowcs Williams-Hawkins (FW-H) equations to predict the acoustic pressure time history and noise spectrum of a helicopter rotor. In this analysis, the acoustic pressure is divided into four components: near-field thickness noise, far-field thickness noise, far-field noise due to blade loading, and near-field noise due to blade loading, which are then combined for a given observer to yield the overall sound pressure. The actual computation is performed by dividing the blades into small panels, determining the retarded time for each panel, and then evaluating the integrals for all the blades for a fixed observer position and time. Repeating this process over discrete time intervals provides the acoustic pressure time history.

RESULTS

High-speed impulsive (HSI) noise was the first noise mechanism to be examined for the doubly-swept blade. From this study, a suitable blade planform which had good HSI features and more acceptable aeroelastic qualities was selected. This blade then served as the starting point for the blade-vortex interaction (BVI) noise study. In this section, results for the HSI- and BVI-noise studies are presented.

The baseline blades for this study are the Black Hawk blade and the baseline doubly-swept blade. The Black Hawk blade is untapered with 20 degrees of aft sweep starting at about 92 percent span. It has SC1095 and SC1095-R8 airfoil sections and a linear twist rate of -13 degrees over most of the blade. There is a "bucket" in the twist near the tip to help alleviate the losses associated with the passing tip vortex in hover (see Figure 8). For the baseline doubly-swept blade, the optimized planform from Ref. 2 (shown in Figure 1) is used but the twist distribution and airfoil sections are those of the Black Hawk blade. Thus the only differences between the Black Hawk blade and baseline doubly-swept blade are the sweep and chord distribution.

High-Speed Impulsive Noise

As discussed previously, the high-speed impulsive noise increases dramatically when the supersonic region relative to the blade-fixed coordinate system extends to the sonic cylinder and this phenomena is called delocalization. The advancing tip Mach number (M_{adv}) at which delocalization occurs is called the delocalizing Mach number, denoted as $M_{delocal}$. The higher the delocalizing Mach number, the faster the helicopter can fly before HSI noise increases greatly and becomes the dominant source of noise. Thus, to improve the HSI-noise characteristics of the blade, the goal is to maximize $M_{delocal}$. The primary objective of this study was to increase the delocalizing Mach number as much as possible over the Black Hawk while maintaining similar aeroelastic characteristics to the original Black Hawk blade (i.e., effective aft sweep). Such a blade would be considered the "best" for the reduction of HSI noise. A secondary objective was to study the impact of unsteady and viscous effects on the prediction of $M_{delocal}$ compared with the earlier quasi-steady full-potential work presented in Ref. 2.

Baseline Study

As an initial assessment of the HSI-noise benefits of the baseline doubly-swept blade, quasi-steady Euler runs were performed at several conditions for the Black Hawk (UH-60A) blade and the baseline doubly-swept blade. In these runs, the advance ratio (μ) and rotational tip Mach number (M_{hov}) were varied and the flow field was tested for delocalization. To provide a representative blade loading, the control settings were set to those of a similar condition run in the DNW model rotor experimental test (Ref. 45-47, run 14.25, $\mu = 0.33$, thrust level of 1g). In the DNW test, a Mach-scaled model Black

Hawk rotor with 176 miniature pressure transducers was used. The test also included measurements of blade dynamics, acoustics and performance.

For the Euler calculations, 162,560 grid points were used including 127 streamwise, 40 spanwise and 32 in the normal direction. On the blade surface, 107x31 points were used. From this computational study, it was verified that the most critical flight-condition parameter influencing delocalization was the advancing tip Mach number. Advance ratio or rotational tip speed could be varied, but as long as the advancing tip Mach number was the same, the state of delocalization would be unchanged. Figure 9 presents a nomograph for advancing tip Mach number and the rotor advance ratio as a function of rotational tip Mach Number and helicopter flight speed (V_∞). Lines of constant advance ratio are given as dashed lines, the solid lines represent lines of constant advancing tip Mach number. Since M_{adv} is the most critical parameter used to identify the onset of delocalization, and rotor advance ratio is an important forward-flight parameter, this nomograph is useful in selecting operational parameters to investigate delocalization boundaries while maintaining realistic operating conditions. The advance ratio is bounded by the onset of dynamic stall, limited to about 0.46 for present-day conventional helicopters. Increasing advance ratio or rotational tip Mach number does not cause delocalization until $M_{adv} = M_{delocal}$. The goal is to modify the tip design to allow an increase in the flight speed without M_{adv} reaching $M_{delocal}$. Several of the conditions studied for the baseline Black Hawk (circles) and baseline doubly-swept geometries (squares) are marked on this figure. The solid symbols indicate conditions at which delocalization occurred. Black Hawk symbols beyond $M_{adv} \cong .890$ and doubly-swept symbols beyond $M_{adv} \cong 0.95$ are in the delocalized region. To maximize the flight speed before delocalization occurs, the condition must be along the line of maximum advance ratio (taken as 0.46). From the results presented in this figure, the use of the baseline doubly-swept tip design is seen to significantly increase $M_{delocal}$ relative to the Black Hawk tip. In addition, $M_{delocal}$ has been increased so much that delocalization does not occur until about 200 knots (for $\mu = 0.46$). The computed $M_{delocal}$ for the Black Hawk blade was found to be between 0.895 and 0.90 based on these unsteady inviscid predictions from NSR3D. (This agrees favorably with the experimentally estimated value of 0.89 for the model Black Hawk rotor.) The baseline doubly-swept blade improved on this value significantly with a $M_{delocal}$ between 0.950 and 0.955.

In Figure 10, contours of relative Mach number are given for the baseline doubly-swept and Black Hawk blades for a condition with $M_{adv} = 0.93$, (μ=0.331, M_{hov}=0.702, run 14.25 of the DNW test described in Refs. 45-47). The difference in the supersonic regions is dramatic and delocalization is evident for the Black Hawk but not the baseline doubly-swept blade.

Unsteady Effects

The earlier work of Refs. 1 and 2 was based on quasi-steady full-potential calculations. Although one would not expect significant differences between full-potential and Euler calculations at these conditions, unsteady effects could be important. Initially, many quasi-steady calculations were performed at several azimuth locations in increments of

five degrees to determine the azimuthal extent of delocalization of the Black Hawk blade. Based on these quasi-steady results for $\mu = 0.33$ and $M_{adv} = 0.93$, delocalization initialized between blade azimuths of 50 and 55 degrees and continued until between 120 and 125 degrees. An unsteady run for this case predicted the onset of delocalization at 61.5 degrees and continuing to 122.5 degrees. Thus the quasi-steady results predicted a slightly larger azimuthal extent of delocalization than the predicted unsteady results. More importantly, one unsteady run automatically determined the entire azimuthal range of delocalization as opposed to running many quasi-steady runs, while providing transient effects which may be of some importance. For this reason, in subsequent studies, unsteady Euler calculations were performed to determine the onset of delocalization.

Viscous Effects

To investigate the effects of viscosity in the prediction of delocalization, a study using the baseline doubly-swept blade design was performed in the viscous quasi-steady mode. Viscous results were compared with quasi-steady inviscid results at a condition where delocalization occurred. For these solutions, the supersonic regions beyond the blade were compared to determine the effect of viscosity. The viscous solutions produced a supersonic region of slightly larger width extending into the far-field than the inviscid results. This result appears to be due to the effective thickening of the blade section due to the boundary layer which strengthens the disturbance in the far-field. This result also indicates that the onset of delocalization would occur at a slightly lower M_{adv} than that predicted by an inviscid solution. Based on the experience gained during this study, the difference is believed to be small from a design point of view, and probably less than 0.005 Mach number. The computational effort to identify the actual $M_{delocal}$ value was believed to be an unwarranted effort and was not pursued any further.

Blade-Geometry Variations

After the initial delocalization studies, a number of changes were made to the baseline doubly-swept blade-tip geometry to determine an acceptable planform which reduces the aeroelastic concerns of the doubly-swept tip but maintains, or possibly improves, the high degree of HSI-noise reduction. These variations included modifying the planform shape by changing the taper ratio and the leading-edge and trailing-edge sweep angles of the swept sections. The purpose of modifying the planform was primarily to produce an effectively aft-swept blade (for aeroelastic reasons) with beneficial delocalization properties but also to determine if the doubly-swept blade could be further improved for high-speed impulsive noise. The effect of the thickness ratio was also studied. Furthermore, BVI-noise reduction, which will be discussed later, may be enhanced by using an airfoil with a sharp leading edge to effect the tip-vortex structure. For this reason, this airfoil-shape variation was also included in the HSI study to insure that this modification does not sacrifice HSI-noise performance.

Aeroelastic stability is an important consideration for these blade geometries. As an approximate measure of the aeroelastic behavior of the blades, an effective sweep of each

blade studied was computed. This effective sweep was found by computing the average location of the quarter-chord line on a thrust-weighted basis. The thrust was assumed to be proportional to the chord and vary linearly with r. From this average quarter-chord line an effective sweep angle can be defined by direct comparison with the same value obtained for a constant-chord aft-swept blade whose sweep starts at the same spanwise location. Although the thrust weighting overly biases the importance of the tip, it does provide a consistent effective measure of relative sweep for comparison purposes. An effectively aft-swept blade was considered to be aeroelastically stable, while an effectively forward-swept blade may be unstable and hence undesirable.

A summary of the blade geometries is provided in Table 1. The modifications to the baseline doubly-swept geometry are identified as *mod1*, *mod2*, etc. For the Black Hawk blade, the sweep begins at 92.9% span. For the doubly-swept blades, the aft-sweep begins at 93.55% span and the forward sweep begins at 96.78%. These were the sweep break-points of the original doubly-swept blade studied in Ref. 2. The first two columns are the fractions of root chord at the second sweep-break point (96.78%) and the tip. For example, a 50% means that the chord has reduced to 50% of the chord at the root. In the last column of this table two values of M_{adv} are given. At the lower M_{adv} value, delocalization did not occur, while at the upper value, it did. The difference between the upper and lower limits in M_{adv} (the tolerance) was narrowed to 0.005. The thickness ratio (t/c), when different from the 9.5% of the SC1095, is varied linearly (inboard to outboard) over the span of the section to scale the airfoil-section profile. Thus, for the cases above, 7.0% is the thickness ratio of the tip. The airfoil-section profile, when different from the SC1095, is a blending of a sharp-leading-edged airfoil and the SC1095. The sharp-leading-edged airfoil used at the tip (shown in Figure 11 with the SC1095 and SC1095-R8) is obtained by replacing the SC1095 section with circular arcs for the upper and lower surfaces. These surfaces are forced to match the slope and position at the maximum thickness location and meet at the leading-edge point of the original profile. The sharp-leading-edged airfoil shown in Figure 11 is only used at the tip. Between 96.78% span (the location where forward sweep begins) and the tip, the airfoils sections are interpolated between the SC1095 airfoil and the sharp-leading-edged airfoil.

For the geometries studied, the baseline doubly-swept planform delayed delocalization the most, with a $M_{delocal}$ of between 0.950 and 0.955. Variations to the airfoil shape, whether in thickness or leading-edge shape, did not have a large effect. The baseline doubly-swept planform appears to be the best from a HSI-noise standpoint, but it is also the most aeroelastically undesirable, based on the effective sweep angle. An increase in taper had a direct benefit on the delocalizing Mach number (note *mod5* through *mod8* in Table 1). The increase in inboard and outboard sweep of *mod9* and *mod10* also helped delay delocalization. The thickness of the blade had a significant benefit for the blade with 80% taper (*mod3* and *mod5*) but had no benefit (within the 0.005 tolerance) for the 50% tapered blade (baseline and *mod1*). The sharp-leading-edged airfoil shape exhibits a benefit for delocalization (*mod3* and *mod4*). The blade geometry labeled *mod10* was selected for further study for the BVI-noise investigation due to its high $M_{delocal}$ of 0.94-

Blade Name	Chord		Sweep			Tip Airfoil		$M_{delocal}$
	0.97R	Tip	Inner	Outer	Effective	t/c	Shape	
B-Hawk	100%	100%	-20.0 °	-20.0 °	-20 °	9.5%	SC1095	.895-.900
Baseline	75%	50%	-19.7 °	+34.1 °	0 °	9.5%	SC1095	.950-.955
Mod1	75%	50%	-19.7 °	+34.1 °	0 °	7.0%	SC1095	.950-.955
Mod2	75%	50%	-34.3 °	+29.5 °	-9 °	7.0%	Sharp LE	.950-.955
Mod3	90%	80%	-34.3 °	+29.5 °	-13 °	7.0%	SC1095	.935-.940
Mod4	90%	80%	-34.3 °	+29.5 °	-13 °	7.0%	Sharp LE	.935-.940
Mod5	90%	80%	-34.3 °	+29.5 °	-13 °	9.5%	SC1095	.925-.930
Mod6	90%	70%	-34.3 °	+29.5 °	-13 °	9.5%	SC1095	.930-.934
Mod7	90%	60%	-34.3 °	+29.5 °	-12 °	9.5%	SC1095	.934-.940
Mod8	90%	50%	-34.3 °	+29.5 °	-11 °	9.5%	SC1095	.937-.940
Mod9	90%	60%	-34.3 °	+34.4 °	-11 °	9.5%	SC1095	.940-.945
Mod10	90%	60%	-34.3 °	+34.4 °	-11 °	7.0%	Sharp LE	.945-.950

Table 1. Predicted onset of delocalization for the baseline doubly-swept blade and modifications to the doubly-swept blade.

0.945 and effective aft sweep of approximately -11 degrees. Note that the Black Hawk blade has an effective aft sweep (as defined herein) of -20 degrees. This selected blade geometry (*mod10*) is referred to as the modified doubly-swept blade with sharp leading edge. The planform of this blade is shown in Figure 1 with the baseline doubly-swept and Black Hawk blades.

Blade-Vortex Interaction Noise

To determine a representative and significant BVI condition, experimental data were used to help define the flight condition to be studied. A case from the DNW test of a pressure-instrumented model Black Hawk rotor (Ref. 45-47) was identified which exhibited a strong, nearly-parallel BVI event. This case was a descent condition with $\mu = 0.176$, $M_{hov} = 0.637$, $\alpha_{tpp} = 5.4$, and $C_L/\sigma = 0.070$. The run number for this case is 11.29. For this study, the thrust was increased to give a 1g value ($C_L/\sigma = 0.090$). In Figure 12, the BVI events for this case, measured in the experiment (Ref. 47), are displayed. The symbols indicate the BVI locations as determined from pressure data at specific blade radial stations. The size of the symbols indicate their relative strengths. Identification of these BVI events was based on the local minima and maxima of the higher harmonic content of the experimental sectional thrust (C_t) obtained from chordwise integration of the pressures. Harmonics greater than four times the blade passage frequency were used for this analysis. Circles are used in this figure at locations of maximum sectional thrust (C_t) and squares are used at locations of minimum C_t. Most of the BVI events occur in the aft region of the rotor disc, the event is particularly strong in the first quadrant at about 40 degrees azimuth. For this study, this event was selected to be modeled. Using the charts from Ref. 44, and interpolating in advance ratio, the origin of the tip vortex

for this interaction was estimated to be 140 degrees. It has been assumed that the blade planform will not affect the location of the originating vortex significantly.

Navier-Stokes solutions were obtained using NSR3D for four blade geometries in this study: the Black Hawk blade, the baseline doubly-swept blade, the modified doubly-swept blade with the sharp leading edge given as *mod10* in Table 1, and a final blade derived from *mod10* called the modified doubly-swept blade with sharp leading edge/new twist. This final blade was designed to increase the loading at the tip to help induce a leading-edge vortex for disruption of the tip vortex. To do this, the twist was increased over the tip region of the blade by two to three degrees. This blade also has the sharp leading edge. In Figure 13, the new twist distribution is compared with the original twist distribution of the Black Hawk blade and the other doubly-swept blades. The twist deviates from the original at about 85 percent span and fairs in smoothly with the inboard twist. It was found that the new twist did not affect $M_{delocal}$ within the tolerance of 0.005.

Navier-Stokes Calculations

To estimate the velocity distribution of the interacting tip vortex, quasi-steady Navier-Stokes calculations were performed for the 140 degrees azimuth location. The solver was used for the outer 50% of the blade. For a spanwise triangular loading distribution, this portion of the blade is expected to carry about 75% of the thrust of a complete blade. Thus the collective was adjusted to trim the computed blade thrust to 75% of that measured by experiment at this azimuth location. For these calculations, 412,160 grid points were used, consisting of 161 streamwise points, 40 spanwise stations and 64 points in the normal direction. On the surface of the blade, 81x31 points were used. The normal spacing of the first point off the blade surface was 0.00007 chords. Behind the trailing-edge, 40 streamwise stations were used to help resolve the convection of the tip vortex. The grids for the doubly-swept blades were stretched to six chords downstream from the *root* trailing edge. For the Black Hawk, the grid was stretched to eight chords downstream of the root trailing edge. These grids provided a maximum downstream distance of six chords from the tip trailing edge. The cut-and-paste assumption was used, specifically, the profiles at these locations were assumed to be the profiles at the location of the blade-vortex interaction. Resolving the tip vortex to the location of the interaction is beyond current state-of-the-art. (Actually, based on the results herein, it could be argued that accurately resolving the tip-vortex formation near the blade tip is beyond today's capabilities.)

These cases were run until the blade thrust was well converged (to the fifth decimal place of thrust coefficient). The loading distributions for the four blades are given in Figure 14. The differences are small except for the modified doubly-swept blade with sharp leading edge/new twist, which has a significantly higher loading at the tip. Note that these blades were trimmed so that the load distributions integrate to within one percent of the same thrust levels. The blades with less loading at the tip have higher loading at the inboard stations. Also, for this particular azimuth location, the loading at the tip is very low. The problem with low tip loading is that there is less of a chance of inducing a leading-edge vortex which is the mechanism which is hypothesized to weaken

the tip-vortex structure. This was the reason for introducing a new blade design with increased twist at the tip. However, even with the increased twist at the tip, the angle of attack at this condition was not large enough to produce a detectable leading-edge vortex at this azimuth location and thrust level. In fact, as a test, the collective was increased by as much as eight degrees, and no detectable leading-edge vortex was produced.

Axial-velocity profiles for the four blades at six chords downstream of the tip trailing edge are shown in Figure 15. These axial velocity profiles are along the straight spanwise line connecting the locations of maximum downwash to maximum upwash in the vertical plane at a specified downstream distance. The vertical planes were taken as parallel to the inboard rotor blade trailing edge. These velocities are nondimensionalized by the freestream speed-of-sound. The distances of the vertical planes are referenced from the blade tip trailing-edge location and nondimensionalized by the inboard blade chord which is the same for all designs. Using the distance from the tip trailing edge provides a measure of the tip-vortex age. The spanwise distances are also nondimensionalized by the chord, and referenced to the tip. Based on these results (Figure 15), the blade which modified the tip-vortex velocity distribution the most (compared with the Black Hawk) is the modified doubly-swept blade with the sharp leading-edge/new twist. It produced a slightly larger peak-to-peak but also increased the core size significantly. The profile for the modified doubly-swept blade with the sharp-leading edge showed little difference in the core region of the vortex from the baseline doubly-swept blade, for this reason it was not analyzed further in this study.

Although these solutions were taken to an adequate convergence tolerance in terms of blade lift, it was later determined that the velocity profiles were not quite fully converged downstream. A convergence history of the velocity profile for the Black Hawk is shown in Figure 16 for six (6) chords downstream of the tip. The number of iterations given in Figure 16 is a cumulative sum of restarting from previous solutions as well as adjusting the collective to trim to the correct thrust coefficient. In all, these runs represent about 150 hours of Cray-2 time. The peak maximum axial velocity appeared to have stopped changing with iteration number, but the core (defined as the distance between the minimum and maximum axial velocities) may still be growing in size. The inboard velocities continue to change slowly indicating a further growth and change in the vortex structure is possible. Due to resource and schedule constraints of the contract, the uncertainty of the time required to obtain true convergence downstream, and some accuracy considerations to be discussed, calculation of completely converged velocity profiles was not pursued further.

BVI Inflow

The axial-velocity profiles predicted by NSR3D were input to the vortex-lattice code, BVI_INFLOW. This analysis then computed the tip-vortex-induced inflow time histories associated with the BVI event of interest at the following blade for the final three blade tip geometries (the Black Hawk, baseline doubly-swept, and modified doubly-swept with sharp leading edge/new twist). In these applications, only the tip vortex which had a parallel

encounter with the blade near the 50 degree azimuth position was used to determine the BVI inflow. In the model, only the vortex segments which had a strong effect on the outer 20% of the blade were used for the interaction. At the location of interaction the velocity profile was assumed to be the same as that six chords downstream of the originating blade. To produce the maximum influence on the blade of interaction, the tip vortex was assumed to impact the blade without local distortion.

The BVI inflow distributions at the tip-path plane are shown in Figures 17 and 18. In Figures 17a-17c, contours of the inflow velocity over the entire rotor tip-path plane, due to the selected BVI vortex segments, are displayed for the three blade geometries. The BVI event is evident in the first quadrant near the edge of the rotor disc. In Figures 18a-18c, the region near the BVI event is enlarged, providing some of the details of the inflow distribution. The general character of the inflow is consistent with the expected inflow for a vortex passage. However, it will be indicated that the amplitudes are too low.

Unsteady Loading

The BVI inflow distributions over the rotor disc, attributable to the BVI vortex segments, were used by NSR3D to predict the unsteady Euler solutions for the final three blade geometries. For these calculations, the same 164k-grid was used. The higher harmonic content (harmonics equal to or greater than 2 blade passage frequencies) of the sectional normal force coefficient are given for the three blades at $y/R = 0.90$ in Figure 19. The BVI event is apparent between 40 and 60 degrees. The sectional load decreases sharply where the downwash is a maximum then increases as the blade passes the maximum upwash due to the vortex. Although the C_n time histories are consistent with the velocity profiles in relative magnitude and time span, these time histories do not provide the impulsive intensity in loads that has been observed for BVI events in experimental data (Ref. 45-47). That is, the duration is too long and the magnitude too small. The suspected reason for this is that the vortex was not realistically predicted, having too great a core size and too small of a peak velocity.

Noise Prediction

The prediction of the acoustic behavior for the final three blade geometries, using the predicted unsteady blade surface pressures from NSR3D, was performed with the WOPWOP analysis. Predicted contours of overall sound pressure level (OASPL) for the rotor with the three blade designs, for a section of a sphere below the rotor at a distance of six rotor radii, are given in Figure 20. The horizontal axis of these figures (θ) is the lateral angle measured from the hub. The lateral angle is defined as zero directly below the hub and increases in the counter-clockwise direction when viewed from behind the helicopter. A lateral angle of 90 degrees is to the right (advancing) side of the helicopter and -90 degrees is to the left. The vertical axis represents the the longitudinal angle from the hub. The longitudinal angle is defined as zero degrees in the direction of the tail and increases in the counter-clockwise direction when viewed from above. A longitudinal angle of 180 degrees is directly in front of the helicopter and 90 degrees is on the advancing side.

The maximum noise level is located on the advancing side slightly in front of the hub at $\theta = 30$ degrees and $\phi = 150$ degrees. The doubly-swept blades produced slightly larger predicted maximum noise levels than the Black Hawk blade (105.8 db for the baseline doubly-swept, 105.6 db for the modified doubly-swept blade with sharp leading edge/new twist, versus 102.7 db predicted for the Black Hawk).

The predicted acoustic signatures for an entire revolution are shown in Figure 21 with the experimental data from the DNW test case 11.29 (mic #9 located at $\theta = 33$ degrees and $\phi = 150$ degrees). An enlarged view of the higher-harmonic content of noise signal is given in Figure 22. Absolute correlations with experiment were not expected since only one feature of the rotor noise was being modeled (i.e. the interaction of the tip vortex with the tip of the following blade). The predictions exhibit some of the characteristics of the experimental BVI-noise signals, but they are not as impulsive and miss a few features. The higher harmonics highlight the BVI signature. The calculations have a wider signal and lower magnitude than the experiment. The differences were determined to be due to the large core size and lower peak velocities of the predicted tip vortex. As mentioned previously, the tip vortex was assumed to pass the blade without any axial displacement (i.e. impact the blade while maintaining its velocity profile). Due to the 1/r decay property of vortex-induced flow, the BVI signature would be even weaker had the vortex passed below the blade, which is usually the case for real blade-vortex interactions. It is important to note that the small differences in the predicted downstream axial velocity profiles (Figure 15) seen between the blades is reflected in the OASPL plots in Figure 20 and the time history plots (Figure 21 and 22). This demonstrates that the unsteady Euler analysis and acoustics code are capable of discriminating between such differences in velocity profile.

Tip-Vortex Resolution

It was previously mentioned that the downstream velocity profiles computed by the Navier-Stokes solver and used for the acoustic analysis were close to, but not completely converged. Upon further investigation and analysis, it was concluded that all of the predicted velocity profiles are not accurate descriptions of the actual tip-vortex structures. A careful study of the dimensional values of the peak-to-peak velocity magnitudes indicated that they were too low, based on experimental observation. In addition, it had been observed earlier in the study that the core size was too large. The degree of convergence of the downstream velocities (Figure 16) appears to be of secondary importance. That is, numerical diffusion of vorticity in the Navier-Stokes solver is the primary problem.

In Figure 23, the development of the tip-vortex axial velocity profile behind the Black Hawk blade tip is shown. The core size decreases as the tip vortex is convected downstream. This is an indication that the vortex roll-up is progressing very slowly. In addition, as the vortex is convected downstream the magnitude of velocity is decreasing, evidence of the numerical dissipation. The peak-to-peak axial velocities at one chord downstream is three times greater than that at six chords downstream. However, it appears that the tip vortex has not yet coalesced at one chord downstream. It is conjectured that the slow

coalescence is due to the peak loading occuring inboard (at about 50% span and shown in Figure 14), resulting in a shallow circulation gradient towards the tip. This loading distribution is due to a combination of the Black Hawk twist distribution and flight condition. Although the velocities are too small close to the blade, the slow coalescence process has allowed additional numerical diffusion to occur before the tip vortex is fully developed.

Due to differences in loading distributions, direct comparisons of the velocity profiles with experiment are difficult. For qualitative comparison purposes, consider the Black Hawk velocity profile at six chords downstream (Figure 15). For a full-scale rotor, the peak-to-peak predicted velocities at this location is about 15 ft/sec and an estimated core diameter of 1.5 chords. This velocity is significantly lower than the expected peak velocity of such a helicopter tip vortex. Typically for this size of a helicopter, peak velocities at the tip vortex are about 100 ft/sec. Additionally, the nominal core diameter of a fully-developed tip vortex has been observed experimentally to be about 1/10 of a chord.

Experimental tip-vortex velocity data is available for another blade geometry in Ref. 61. The baseline geometry for this experiment had a 32% taper ratio, starting at 75% span, and Boeing VR-12 airfoil sections. Induced downwash angles of the tip vortex are shown in Figure 25 for a blade with a wing lift coefficient of 0.5. Based on this figure, the core size is about 1 inch, which is 0.31c based on the chord at the tip and 0.10c based on the root chord. The peak-to-peak induced angles, from Figure 25, are 16 degrees. For comparison, the Navier-Stokes calculations shown in Figure 16 have peak-to-peak induced angles of about 4 degrees at two chords downstream and decreased to 1.5 degrees at six chords downstream. Although these comparisons are considered qualitative due to differences in geometry and blade loading, the computed values are apparently too weak. The difference in velocity magnitudes between two chords and six chords downstream indicate the rapid numerical diffusion of the vortex.

The predicted tip vortex, due to spanwise grid size, numerical diffusion, and artificial dissipation, is much too weak and broad. A very fine, preferably adaptive, grid is needed to resolve the tip vortex far enough downstream to be fully developed. Studies are required using higher-order, up-winded numerical schemes (Ref. 34) and/or grid refinement (Ref. 35) to improve the resolution of the tip vortex and determine whether it can be computed adequately for noise prediction. Although it was anticipated at the onset of this study that the artificial and numerical dissipation would affect the results, the degree of impact was not expected due to several reasons. The tip vortex structure developed further downstream than anticipated, allowing the diffusion to be more significant. The blade-tip loading for the condition studied was very low, producing a weak tip-vortex and no leading-edge vortex to disrupt the flow. It had been conjectured that large enough differences in the tip-vortex flow would be present, due to the formation of a leading-edge vortex, such that relative comparisons between the flow-fields would be realistic despite the presence of numerical diffusion. Without these large differences, the flow-solver could not reliably distinguish the tip-vortex profiles. As such, within the available computer resources, the tip-vortex structure could not be predicted accurately enough to use the results for noise prediction.

CONCLUSIONS

Rotor blades with doubly-swept tip designs, specifically inboard aft-swept and outboard forward-swept, were shown to significantly delay the onset of delocalization relative to the aft-swept Black Hawk rotor blade, as expected. These results for several doubly-swept tip designs are based on predictions from a Euler/Navier-Stokes rotor flow code, NSR3D, and confirmed the results of an earlier NASA study on a doubly-swept geometry using a quasi-steady full-potential method. The prediction of the advancing tip Mach number at which the Black Hawk blade exhibited delocalization agreed well with the experimental observation of 0.89 for the model Black Hawk rotor. The investigation demonstrated, on a limited basis, that unsteady and viscous effects do not significantly alter the prediction of the delocalization boundaries. Starting with the baseline doubly-swept tip design which had an effective forward sweep based on the thrust-weighted location of the blade quarter-chord line and a $M_{delocal}$=0.95, a new doubly-swept tip planform was developed by analysis of the delocalization boundaries of several variations of the baseline geometry. The new planform retained the inboard aft sweep and outboard forward sweep features, and had similar delocalization benefits. Delocalization occurred at an advancing tip Mach number of 0.94, but the blade had an effective aft sweep to reduce the possibly undesirable aeroelastic behavior of the baseline doubly-swept tip. Both of the these doubly-swept blades retained the airfoil and twist distributions of the Black Hawk. These studies indicate the potential of the doubly-swept tip to allow a helicopter rotor to fly at speeds over 200 knots without delocalization and thus demonstrate the potential of such tip designs to reduce HSI noise.

A procedure for the prediction of tip-vortex structure and its effect on BVI noise was developed. The method is based on a loose coupling of steady Navier-Stokes, vortex-lattice, unsteady Euler, and linear acoustic methodologies. This methodology was employed to investigate the potential of the doubly-swept tip to alter the tip-vortex structure in a manner which would reduce BVI noise in the first quadrant of the rotor disk. The results of this study were inconclusive due to the inability of the Navier-Stokes flow solver to predict realistic tip-vortex velocity distributions downstream of the blade tip within acceptable computer resource constraints. The predicted peak-to-peak velocities were too small and the vortex core sizes too large due to greater than anticipated numerical diffusion effects. The severity of the diffusion effects were partly due to the large distance required for the tip vortex to form at the condition studied. In addition, for the low blade-tip loadings on the advancing side, the forward-swept portion of the tip, even with the sharp leading edge at the extreme tip, did not produce a leading-edge vortex which was hypothesized to be the mechanism which would alter the tip-vortex structure. Thus, a weakening of the tip vortex did not occur, and the Navier-Stokes code did not predict significantly different tip-vortex velocity profiles for the different blades. The prediction procedure did predict differences in the noise, although it is not clear whether these differences are due to blade geometry or the BVI-induced inflow. The procedure may prove to be a useful tool when the difficulties of predicting realistic tip-vortex structures can be overcome, or by using experimental tip-vortex velocity data for different tip geometries.

SUGGESTIONS FOR FUTURE RESEARCH

It was shown numerically that the doubly-swept blade delayed the onset of delocalization and thus offers the potential for a significant reduction of high-speed impulsive noise. It is recommended that such a tip design be tested experimentally to determine if the benefits for HSI noise can be realized. Although the investigation of the doubly-swept blade for BVI-noise reduction is inconclusive, this blade should be studied further to determine its potential for BVI noise and its impact on rotor performance and aeroelastic stability.

For the computational analysis of BVI noise to be successful, the calculation of the downstream velocity distribution must be reliable enough for comparisons between blade geometries. During this computational study, it was found that the resolution of the tip vortex was not accurate. A computational study focused on capturing this flow structure is needed. This study could include refinement of the spanwise gridding and improvement of the present methodology, or application of a more sophisticated algorithm (e.g., Refs. 34 and 35). For validation, a comparison with available experimental velocity data is desirable. Since the present numerical method is not capable of adequately predicting the downstream vorticity distributions, an experimental test is needed to determine the effectiveness of the doubly-swept blade for redistributing the downstream velocity field. This would test the underlying premise for using the doubly-swept blade to reduce BVI noise. Additionally, the experimental velocity profiles could be used for the BVI-noise methodology described in this report.

Another useful computational study would address the flow-field at the blade. The original hypothesis for BVI-noise reduction was based on the assumption that the doubly-swept design could redistribute vorticity by causing a leading-edge vortex. For the BVI event studied, the tip loading was very low, making a leading-edge vortex formation difficult. Modifications to the blade section and twist were used as an attempt to trigger the vortex formation, but none of the blade geometries produced a leading-edge vortex at this flight condition. A numerical study to determine what geometry changes are necessary to form the leading-edge vortex at these conditions would be useful. For BVI events which occur at other locations on the rotor disc, such as the retreating side, the origin of the tip vortex may be in a region of high loading. Hence, to suppress the noise associated with these events, a leading-edge vortex may be more likely to form and the doubly-swept blade may offer real potential. Thus, investigation of the greater potential of the doubly-swept tip to produce a leading-edge vortex on the retreating side, and thereby reduce BVI noise, is recommended.

REFERENCES

1. Tauber, M.E., "Computerized Aerodynamic Design of a Transonic Low-Noise Blade"' NASA TM 85928, March 1984.

2. Tauber, M.E., and R.G. Langhi, "Transonic Rotor Tip Design Using Numerical Optimization", NASA TM 86771, October 1985.

3. Schmitz, F.H., Yu, Y.H., "Helicopter Impulsive Noise: Theoretical and Experimental Status," International Symposium on Recent Advances in Aerodynamics and Aeroacoustics, Stanford University, August 1983.

4. Schultz,K-J. and W.R. Splettstoesser, "Prediction of Helicopter Rotor Impulsive Noise Using Measured Blade Pressures", Proceedings of the 43rd Annual Forum of the American Helicopter Society, St Louis, MO, May 1987.

5. Ziegenbein, P.R., and B.K. Oh, "Blade-Vortex Interaction Noise Predictions Using Measured Blade Surface Pressures", Presented at the American Helicopter Specialist's Meeting on Aerodynamics and Aeroacoustics, Ft. Worth, TX, February 1987.

6. Joshi, M.C., Liu, S.R., and Boxwell, D.A., "Prediction of Blade-Vortex Interaction Noise Using Measured Blade Pressures," Presented at the AIAA 11th Aeroacoustics Conference, Palo Alto, October 1987.

7. Visintainer, J.A., Marcolini, M.A., Burley, C.L., and Liu, S.R., "Acoustic Predictions Using Measured Pressures from a Model Rotor in the DNW," Proceedings of the 47th Annual Forum of the American Helicopter Society, Phoenix, AZ, May 1991.

8. Schwindt, C.J. and J.M. Fitzgerald, "A Comparison of Acoustic Predictions with Model Rotor Test Data from the NASA 14' X 22' Wind Tunnel", Proceedings of the 44th Annual Forum of the American Helicopter Society, Washington, D.C., June 1988.

9. Rawls, J.W., "Introduction to the Use of ROTONET", Kentron International, Inc. publication, February 1985.

10. Schwindt, C.J., "ROTONET Noise Prediction Program Capability Development and Procedures for Its Use", NASA CR 178412, December 1987.

11. Egolf, T.A., and A.J. Landgrebe, "Generalized Wake Geometry for a Helicopter Rotor in Forward Flight and Effect of Wake Deformation on Airloads," Proceedings of the American Helicopter Society 40th Annual Forum, Washington, D.C., May 1984.

12. Egolf, T.A., and A.J. Landgrebe, "Helicopter Rotor Wake Geometry and Its Influence in Forward Flight - Volume I - Generalized Wake Geometry and Wake Effects on Rotor Airloads and Performance," NASA CR-3726, October 1983.

13. Marcolini, M.A., Martin, R.M., Lorber, P.F., and Egolf, T.A., "Prediction of BVI Noise Patterns and Correlation with Wake Interaction Locations," Proceedings of the American Helicopter Society 48th Annual Forum, Washington, D.C., June 1992.

14. Bliss, D.B., L. Dadone, and D.A. Wachpress, "Rotor Wake Modeling For High Speed Flows", Proceedings of the American Helicopter Society 43rd Annual Forum , St Louis, MO, May 1987.

15. Egolf, T.A.,"Helicopter Free Wake Predictions of Complex Wake Structures Under Blade-Vortex Interaction Operating Conditions", Proceedings of the American Helicopter Society 44th Annual Forum, Washington, D.C., June 1988.

16. Berry, J.D., "A Multi-Element Vortex Lattice Method for Calculating the Geometry and effects of a Helicopter Rotor wake in Forward Flight", AIAA-88-0664, AIAA 26th Aerospace Sciences meeting, Reno NV, January 1988.

17. Egolf, T.A., and J.P. Massar, "Helicopter Free Wake Implementation On Advanced Computer Architectures", Presented at The 2nd International Conference on Basic Rotorcraft Research, University of Maryland, College park, Maryland, February 1988.

18. Egolf, T.A., and Sparks, S.P., "Hovering Rotor Airload Prediction Using a Full Potential Flow Analysis with Realistic Wake Geometry," Proceedings of the American Helicopter Society 41st Annual Forum, Ft. Worth, TX, May 1985.

19. Egolf, T.A., and Sparks, S.P., "A Full Potential Flow Analysis With Realistic Wake Influence for Helicopter Rotor Airload Prediction. NASA CR 4007, January 1987.

20. Caradonna, F.X., Tung, C., and Desopper, A., "Finite Difference Modeling of Rotor Flows Including Wake Effects," *Journal of the American Helicopter Society*, Vol. 27, No. 2, April 1984.

21. Chang, I-C, and Tung, C., "Numerical Solution of the Full-Potential Equation for Rotors and Oblique Wings Using a New Wake Model," AIAA 85-0268, Presented at the AIAA 23rd Aerospace Sciences Meeting, January 1985.

22. Strawn, R.C., and Caradonna, F.X., "Numerical Modeling of Rotor Flows with a Conservative Form of the Full-Potential Equations," AIAA 86-0079, Presented at the AIAA 24th Aerospace Sciences Meeting, January 1986.

23. Ramachandran, K.,Tung, C., and F.X., Caradonna, "The Free-Wake Prediction of Rotor Hover Performance Using a Vortex Embedding Method," AIAA 89-0638, Presented at the AIAA 27th Aerospace Sciences Meeting, January 1989.

24. Hassan, A.A., and B.D. Charles, "Simulation of Realistic Rotor Blade-Vortex Interactions Using a Finite-Difference Technique", AIAA 89-1847, AIAA 20th Fluid Dynamics, Plasma Dynamics, and Lasers Conference, Buffalo, NY, June 1989.

25. Arieli, R., and Tauber, M.E., "Analysis of the Quasi-Steady Flow About an Isolated Lifting Helicopter Rotor Blade", IAA TR-24, August 1979.

26. Roberts, T.W., and Murman, E.M., "Solution Method for a Hovering Helicopter Rotor Using the Euler Equations," AIAA 85-0436, Presented at the AIAA 23rd Aerospace Sciences Meeting, January 1985.

27. Sankar, N.L., Wake, B.E., and Lekoudis, S.G., "Solution of the Unsteady Euler Equations for Fixed and Rotor Wing Configurations," AIAA 85-0120, Presented at the AIAA 23rd Aerospace Sciences Meeting, January 1985.

28. Chang, I-C., and C. Tung, "Euler Solution of the Transonic Flow for a Helicopter Rotor", AIAA 87-0523, Presented at the AIAA 25th Aerospace Sciences Meeting, January 1987.

29. Agarwal, R.K. and J.E. Deese, "An Euler Solver for Calculating the Flowfield of a Helicopter Rotor in Hover and Forward Flight", Presented at the 19th Fluid Dynamics, Plasma Dynamic, and Laser Conference, Honolulu, HA, June 1987.

30. Srinivasan, G.R., and W.J. McCroskey, "Unsteady Interaction of a Rotor With a Vortex", AIAA 89-1848, AIAA 20th Fluid Dynamics, Plasma Dynamics, and Lasers Conference, Buffalo, NY, June 1989.

31. Wake, B.E., and N.L. Sankar, "Solution of the Navier-Stokes Equations for the Flow About a Rotor Blade", *Journal of the American Helicopter Society* , Vol. 32, No. 2, April 1989.

32. Wake, B.E., and T.A. Egolf, "Implementation of a Rotary-Wing Three-Dimensional Navier-Stokes Solver on a Massively Parallel Computer", AIAA 89-1939, AIAA 9th Computational Fluid Dynamics Conference, Buffalo, NY, June 1989; *AIAA Journal*, Vol. 29, No. 1, Jan. 1991.

33. Wake, B.E., and T.A. Egolf, "Application of a Rotary-Wing Flow Solver on a Massively Parallel Computer", AIAA 90-0334, Presented at the AIAA 28th Aerospace Sciences Meeting, Reno, NV, Jan. 1990.

34. Srinivasan, G.R., Raghavan, V., and Duque, E.P.N., "Flowfield Analysis of Modern Helicopter Rotors in Hover by Navier-Stokes Method," Proceedings for the International Technical Specialists' Meeting on Rotorcraft Acoustics and Rotor Fluid Dynamics, Philadelphia, PA, October 1991.

35. Strawn, R.C., Barth, T.J., "A Finite-Volume Euler Solver for Computing Rotary-Wing Aerodynamics on Unstructured Meshes," Proceedings of the 48th American Helicopter Society Annual Forum, Washington, DC, June 1992.

36. Shenoy, R.K., "Aeroacoustic Flowfield and Acoustics of a Model Helicopter Tail Rotor at High Advance Ratio", Proceedings of the 45th American Helicopter Society Annual Forum, Boston, MA, May 1989.

37. Ashworth, J., Huyer, S., and M. Luttges, "Comparisons of Unsteady Flow Fields About Straight and Swept Wings Using Flow Visualization and Hot-Wire Anemometry", AIAA 87-1334, Presented at the AIAA 19th Fluid Dynamics, Plasma Dynamic, and Laser Conference, Honolulu, HA, June 1987.

38. Simonich, J., McCormick, D., and Lavrich, P., "Interaction Noise Mechanisms for Advanced Propellers Experimental Results", AIAA 89-1093, Presented at the AIAA 12th Aeroacoustics Conference, San Antonio, TX, April 1989.

39. Simonich, J., McCormick, D., and Lavrich, P., "The Role of Leading Edge Vortex Flows in Prop-Fan Interaction Noise," AIAA Paper No. 90-3977, Presented at the AIAA 13th Aeroacoustics Conference, Tallahassee, FL, October 1990.

40. George, A.R. and A.S. Lyrintzis, "Mid-Field and Far-Field Calculations of Blade-Vortex Interactions", AIAA 86-1854, Presented at the AIAA 10th Aeroacoustic Conference, Seattle, WA, July 1986.

41. George, A.R. and A.S. Lyrintzis, "Acoustics of Transonic Blade-Vortex Interactions", *AIAA Journal*, Vol. 26, No. 7, July 1988.

42. Isom, M., T.W. Purcell, and R.C. Strawn, "Geometrical Acoustics and Transonic Helicopter Sound", AIAA 87-2748, Presented at the AIAA 11th Aeroacoustics Conference, October 1987.

43. Purcell, T.W., R.C. Strawn, and Y.H. Yu, "Prediction of High-Speed Rotor Noise With a Kirchhoff Formula", Presented at the American Helicopter Society Specialists Meeting on Aerodynamics and Aeroacoustics, Ft. Worth, TX, February 1987

44. Egolf, T. A. and A. J. Landgrebe, "Helicopter Rotor Wake Geometry and Its Influence in Forward Flight," Volume II - Wake Geometry Charts, NASA-3727, October 1983.

45. Lorber, P.F., "Pressure-Instrumented Model UH-60A Black Hawk Rotor Test at DNW," Volumes I - Description of Experiment, UTRC Report, R91-153577-1, February 1991.

46. Lorber, P.F., "Pressure-Instrumented Model UH-60A Black Hawk Rotor Test at DNW," Volumes II - Contour Plots and Tabulated Data, UTRC Report, R91-153577-2, February 1991.

47. Lorber, P.F., "Blade-Vortex Interaction Data Obtained from a Pressure-Instrumented Model Rotor at the DNW," Proceedings of the AHS International Technical Specialists' Meeting on Rotorcraft Acoustics and Rotor Fluid Dynamics," Philadelphia, PA, October 1991.

48. Beam, R. and Warming, R.F., "An Implicit Factored Scheme for the Compressible Navier-Stokes Equations," *AIAA Journal*, Vol. 16, No. 4, April 1978.

49. Pulliam, T.H. and Steger, J.L., "Implicit Finite-Difference Simulations of Three-Dimensional Compressible Flow," *AIAA Journal*, Vol. 18, No. 2, February 1980.

50. Rizk, Y.M. and Chausee, D.S., "Three-Dimensional Viscous-Flow Computations Using a Directionally Hybrid Implicit/Explicit Procedure," AIAA Paper 83-1910, Presented at the, 1983.

51. Sankar, L.N. and Tang, W., "Numerical Solution of Unsteady Viscous Flows with an Impinging Shock," *AIAA Journal*, Vol. 14, No. 2, Feb. 1976.

52. Tannehill, J.C., Holst, T.L., and Rakish, J.V., "Numerical Computations of Two-Dimensional Viscous Blunt Body Flows with an Impinging Shock," *AIAA Journal*, Vol. 14, No. 2, Feb. 1976.

53. Pulliam, T.H., and Chausee, D.S., "A Diagonal Form of an Implicit Approximate-Factorization Algorithm," *Journal of Computational Physics,* Vol. 39, 1981, pp. 347-363.

54. Simpson, L.B., and Whitfield, D.L., "Finite-Difference Split Algorithm for Unsteady Thin-Layer Navier-Stokes Solutions," AIAA Paper 89-1939-CP, AIAA 9th Computational Fluid Dynamics Conference, Buffalo, NY, 1989.

55. Jameson, A.J., Schmidt, W., and Turkel, E., "Numerical Solutions of the Euler Equations by Finite-Volume Method Using Runge-Kutta Time-Stepping Schemes," AIAA Paper 81-1259, 1981.

56. Baldwin, B.S., and Lomax, H., "Thin-Layer Approximation and Algebraic Model for Separated Turbulent Flows," AIAA Paper 78-257, June 1978.

57. Gee, K., Cummings, R.M., and Schiff, L.B., "Turbulence Model Effects on Separated Flow About a Prolate Spheroid," *AIAA Journal,* Vol. 30, No. 3, March 1992, pp. 655-664.

58. Davis, R.L., Hobbs, D.E., and Weingold, H.D., "Prediction of Compressor Cascade Performance Using a Navier-Stokes Technique," *Journal of Turbomachinery, Transactions of the ASME,* Vol. 110, pp. 520-531, Oct 1988.

59. Degani, D., and Schiff, L.B. "Computation of Turbulent Supersonic Flows Around Pointed Bodies Having Crossflow Separation," *Journal of Computational Physics,*Vol. 66, No. 1, Sept. 1986, pp 173-196.

60. Brentner, K.S., "A Prediction of Helicopter Rotor Discrete Frequency Noise for Three Scale Models Using a New Acoustics Program," Presented at the AIAA 25th Aerospace Sciences Meeting, January 1987.

61. Carlin, G., Dadone, L., and Spencer, R., "Results of an Experimental Investigation of Blade Tip Vortex Modification Devices," NASA CR 181853, June 1989.

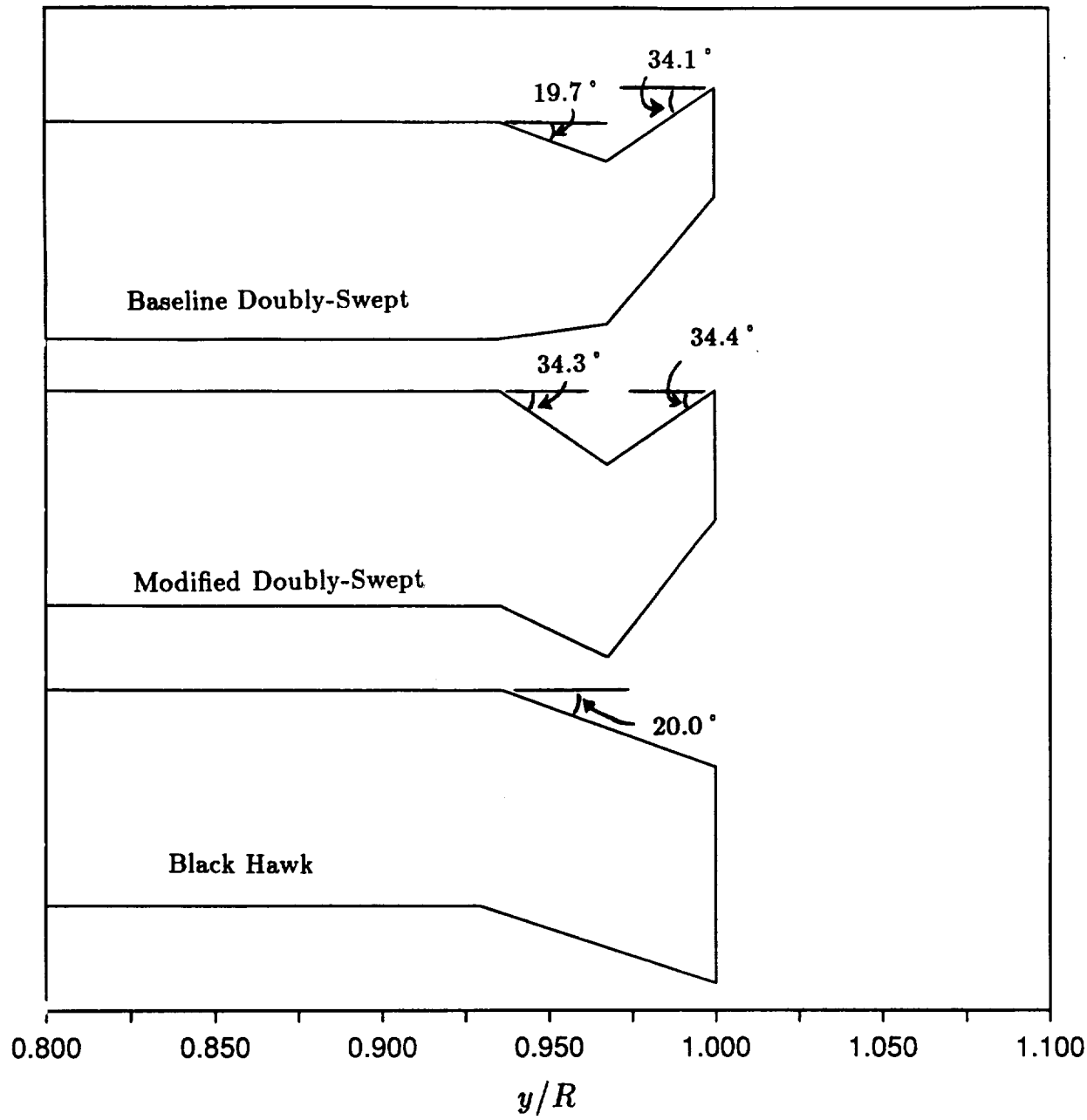

Figure 1. Comparison of blade planforms: baseline doubly-swept blade of Ref. 2, modified doubly-swept blade, and Black Hawk blade

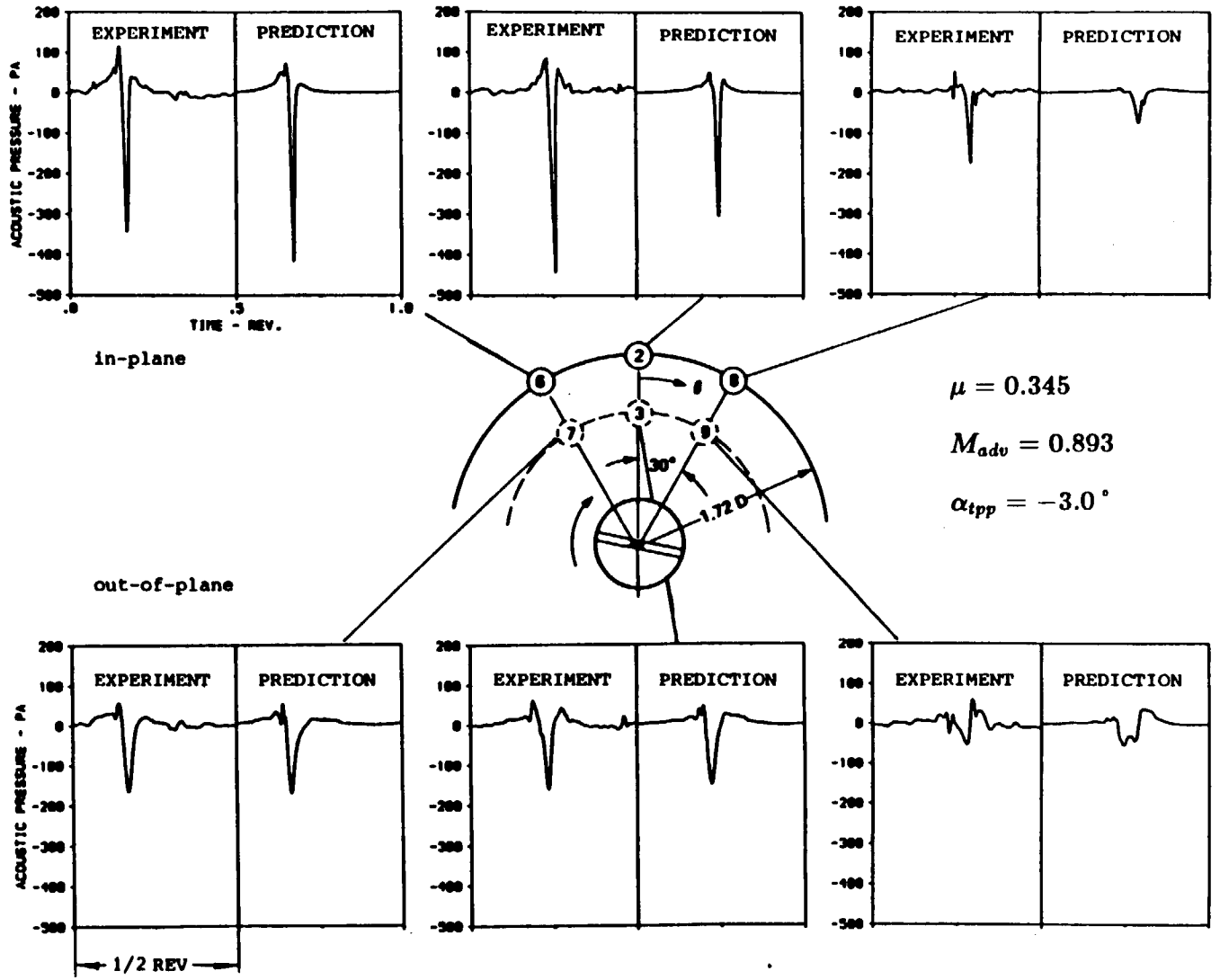

Figure 2. Comparison of experimental impulsive noise and predicted impulsive noise using measured pressure distributions (Ref. 4).

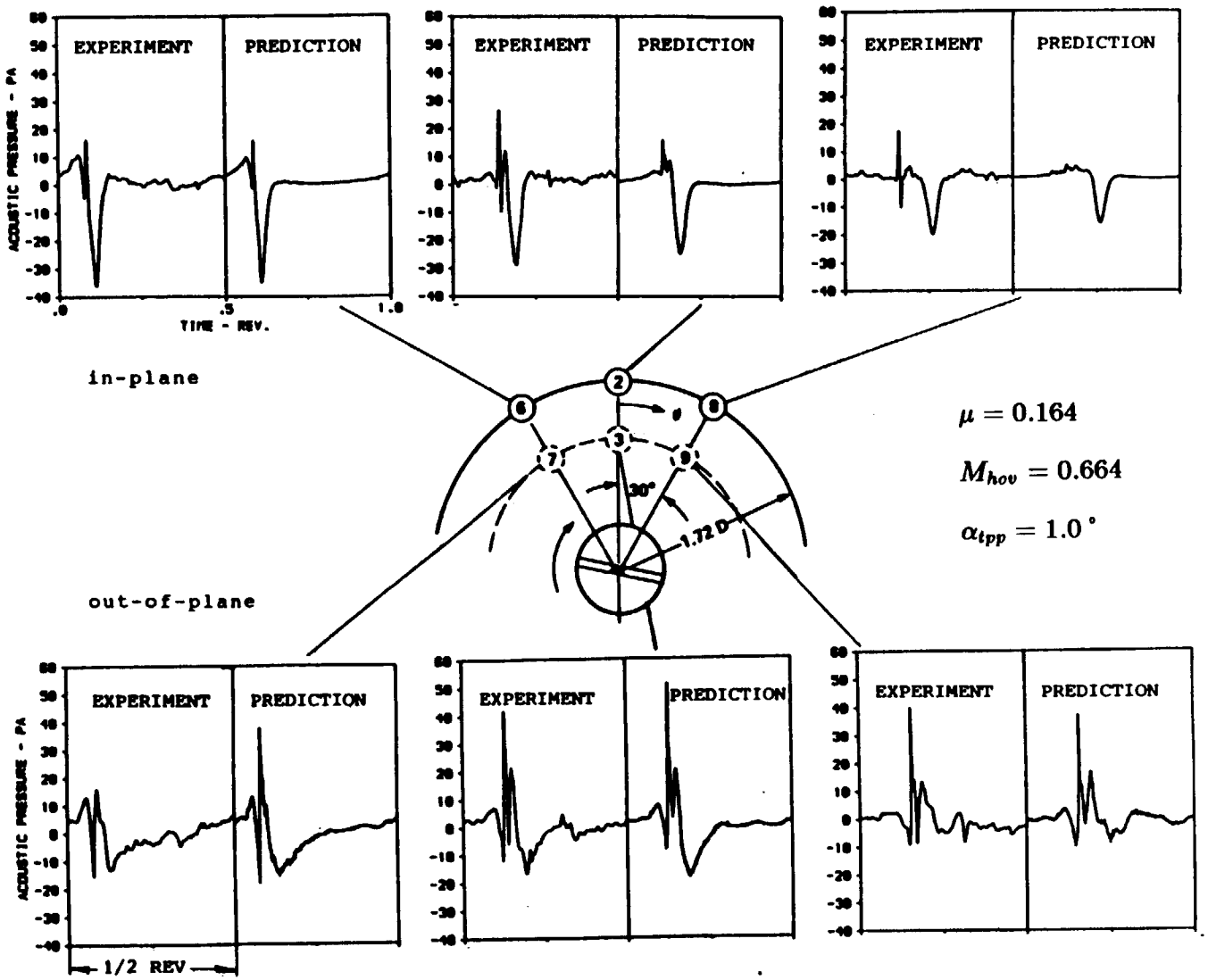

Figure 3. Comparison of experimental BVI noise and predicted BVI noise using measured pressure distributions (Ref. 4).

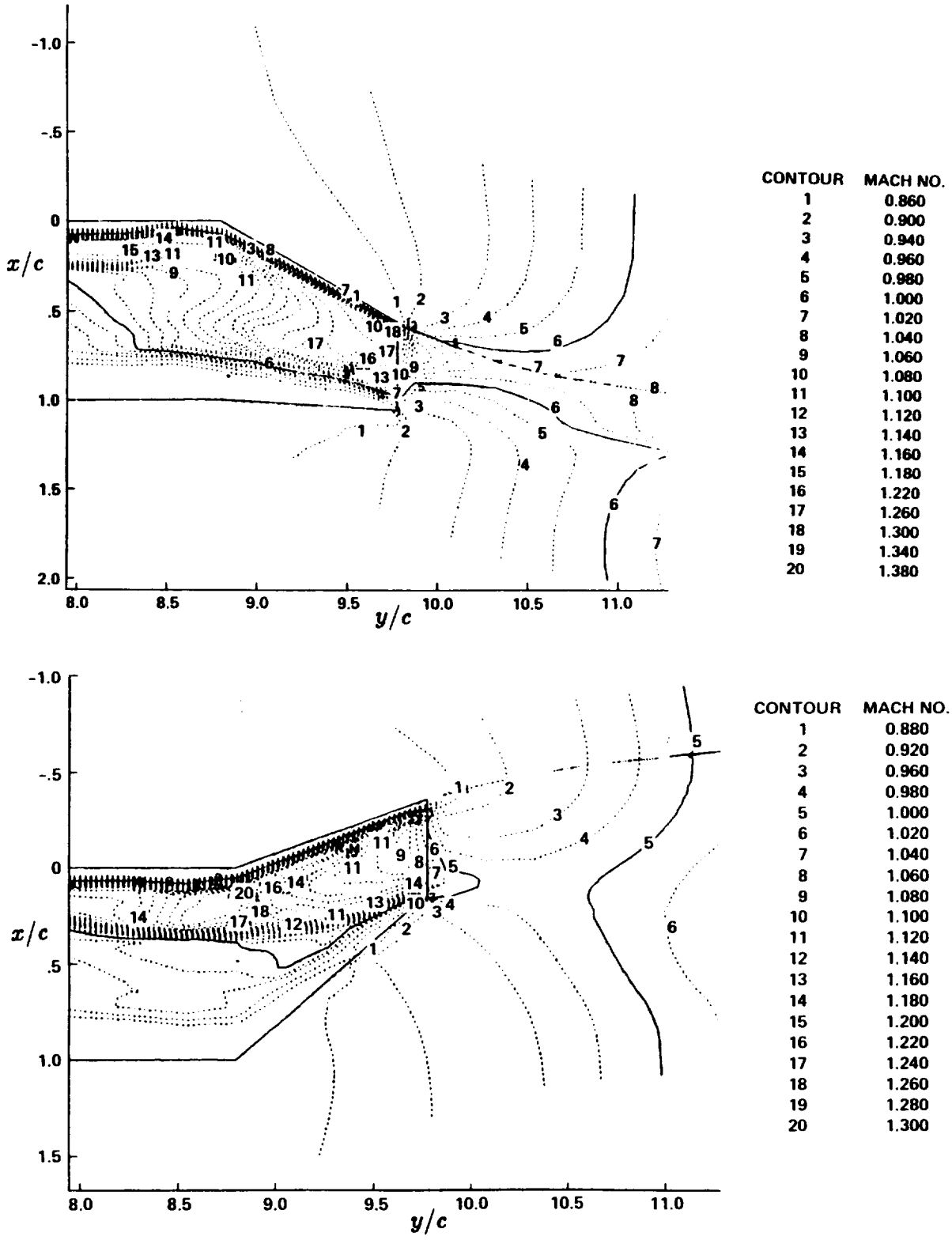

Figure 4. Comparison of predicted upper-surface Mach number contours of aft-swept and forward-swept blade-tip designs (Ref. 1) for M_{adv}=0.92 (μ = 0.41, M_{hov} = 0.65).

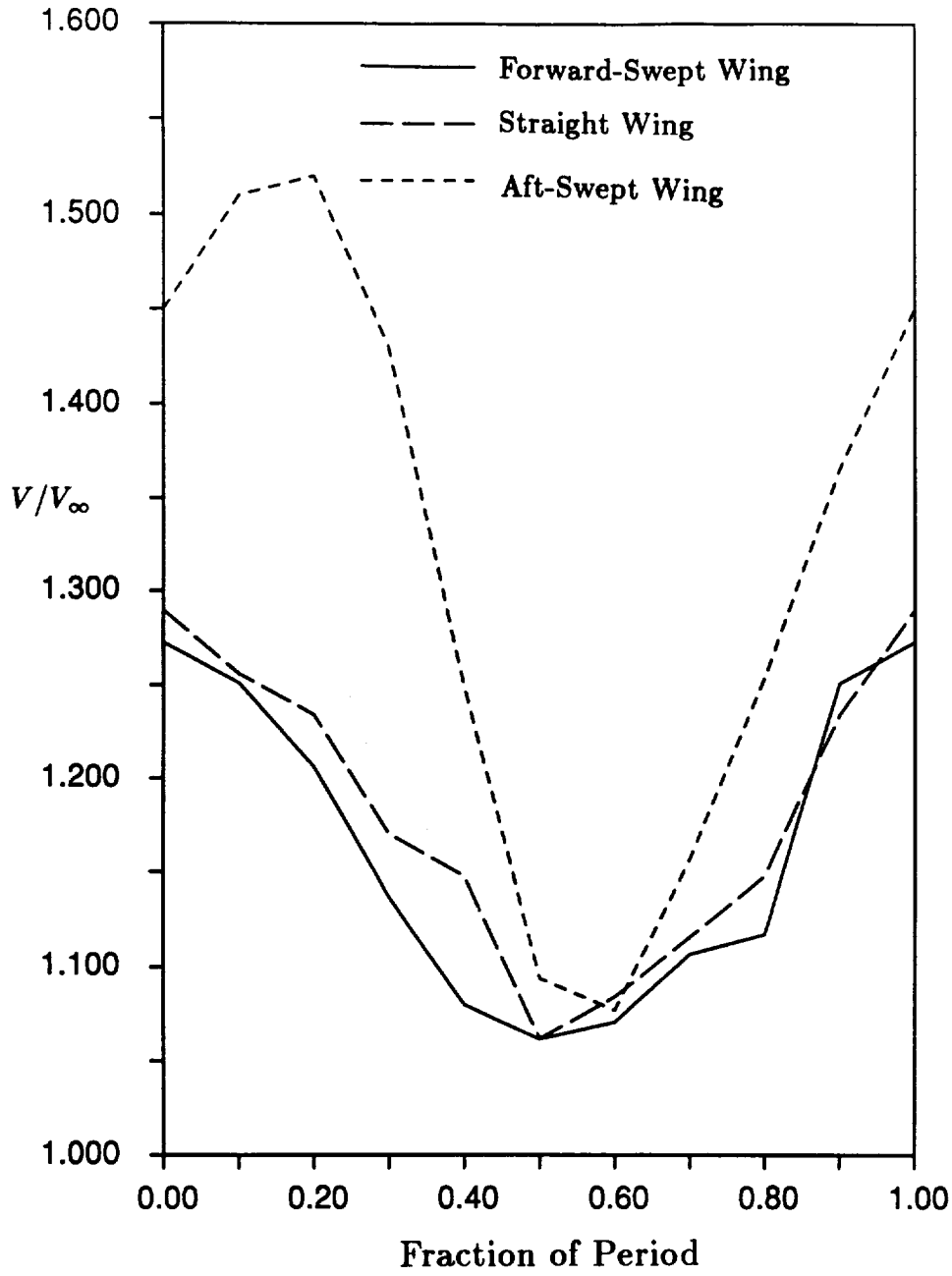

Figure 5. Measured velocity at a point 0.10 chords above of the tip and 0.17 chords downstream of the leading-edge for oscillating forward-swept, straight, and aft-swept wings (Ref. 37).

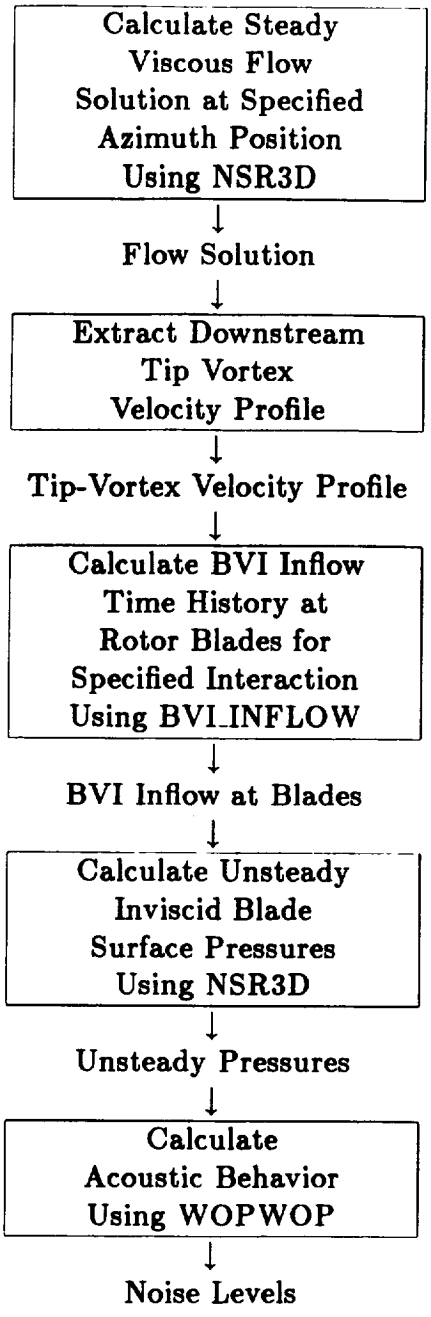

Figure 6. Flow-chart of the coupled methodology for BVI noise prediction.

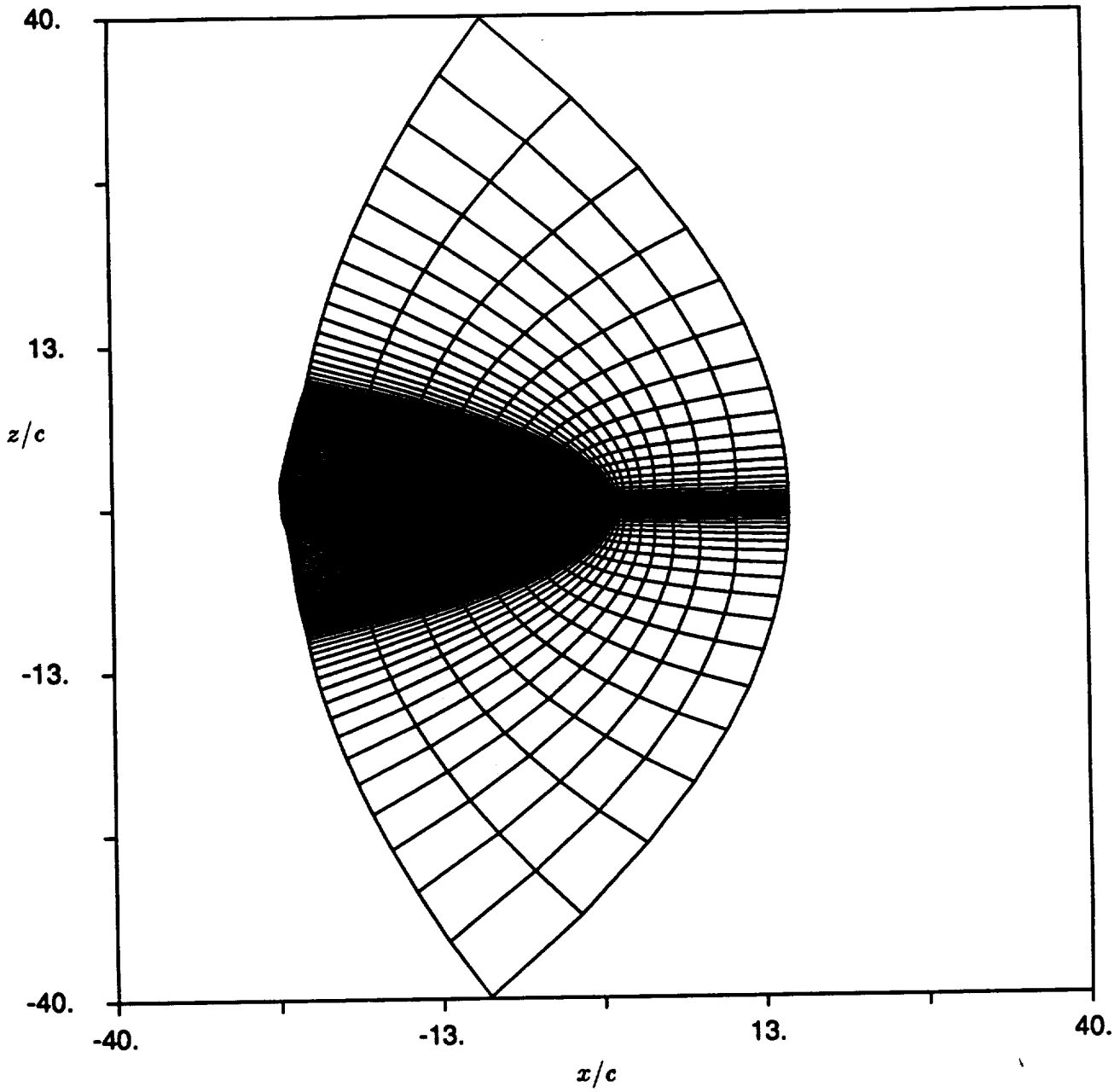

Figure 7a. C-grid geometry in a spanwise plane used for the Euler calculations.

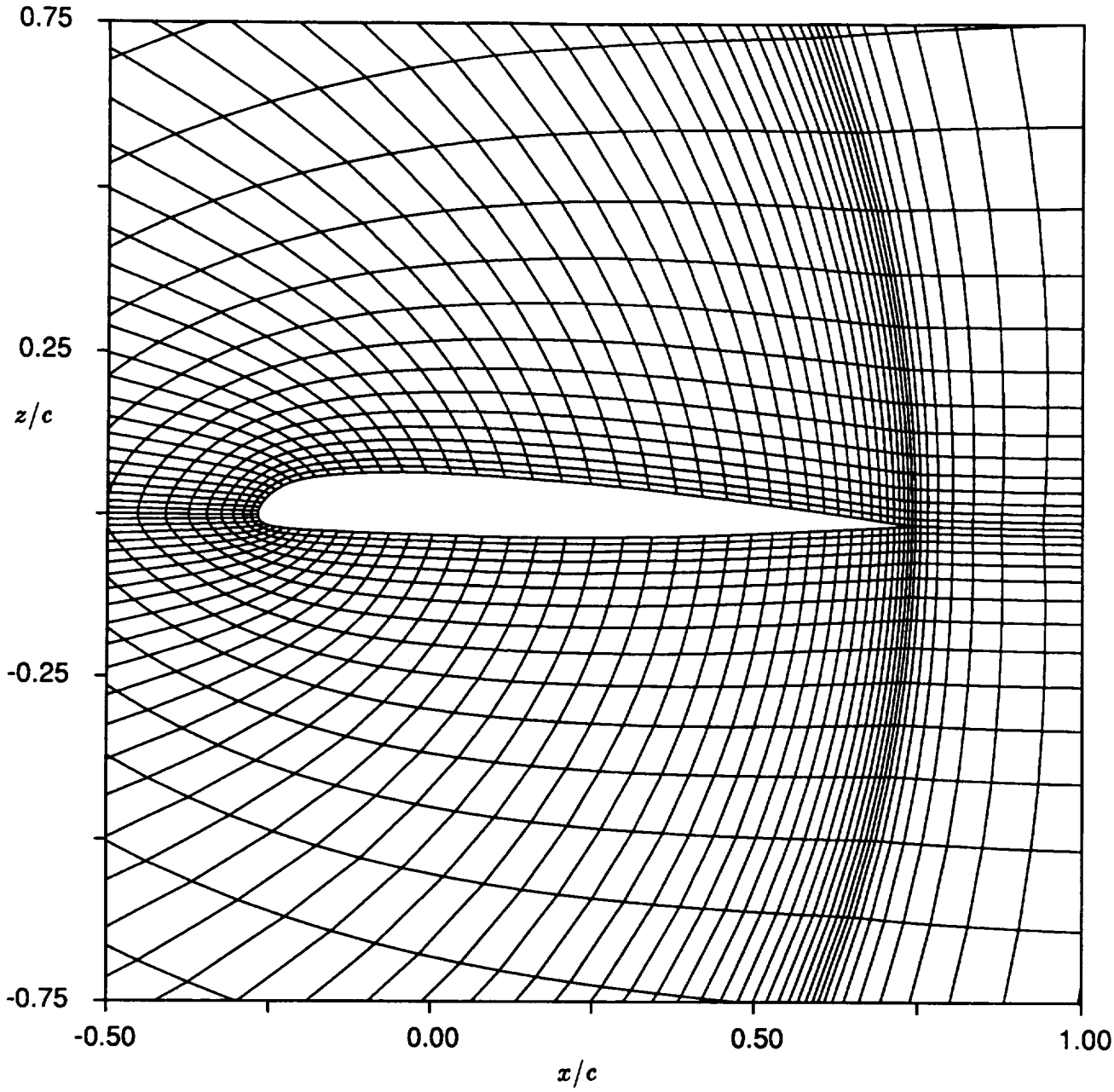

Figure 7b. Close-up view of C-grid geometry in a spanwise plane used for the Euler calculations.

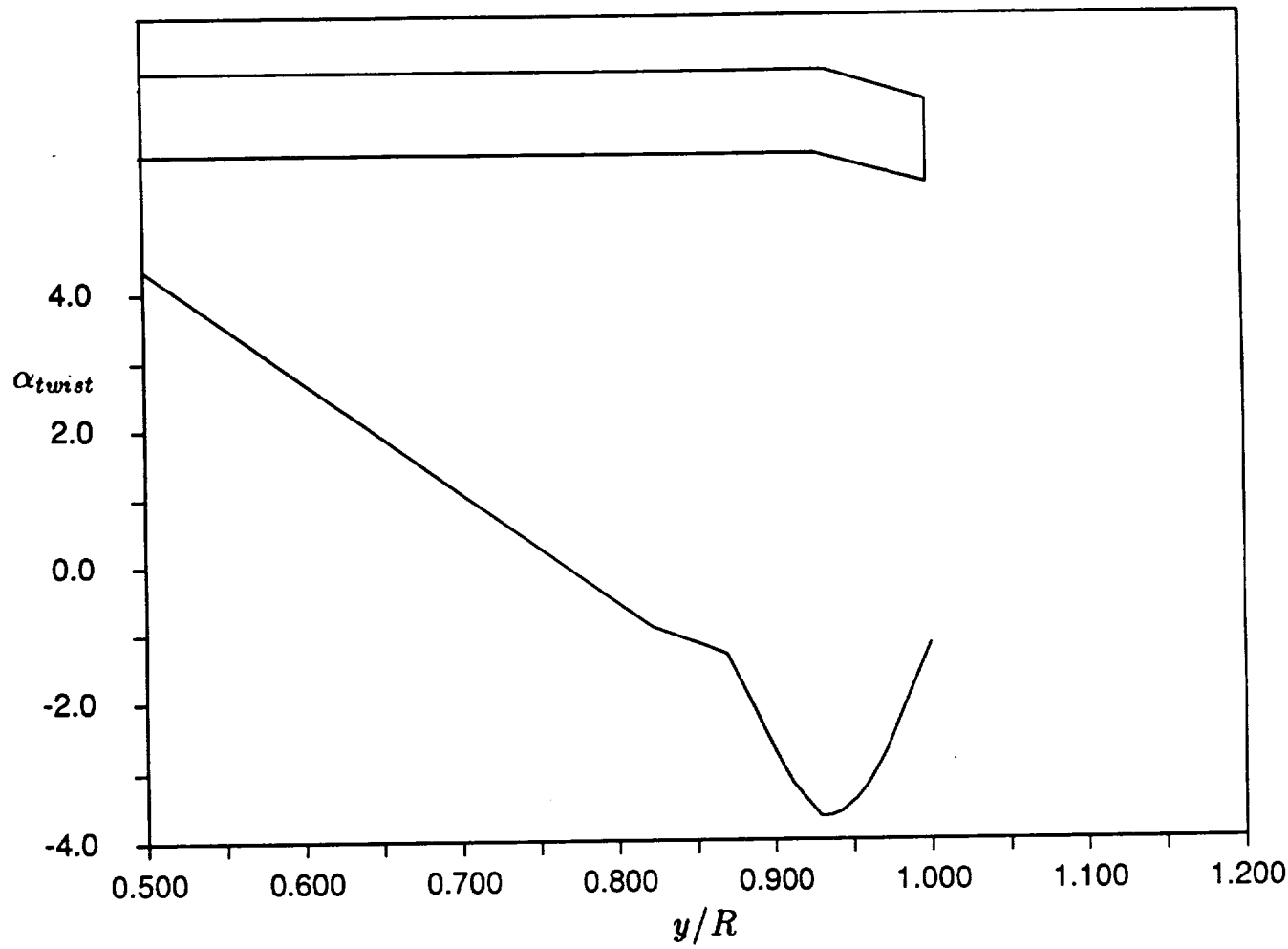

Figure 8. Twist distribution shown with blade planform for Black Hawk blade.

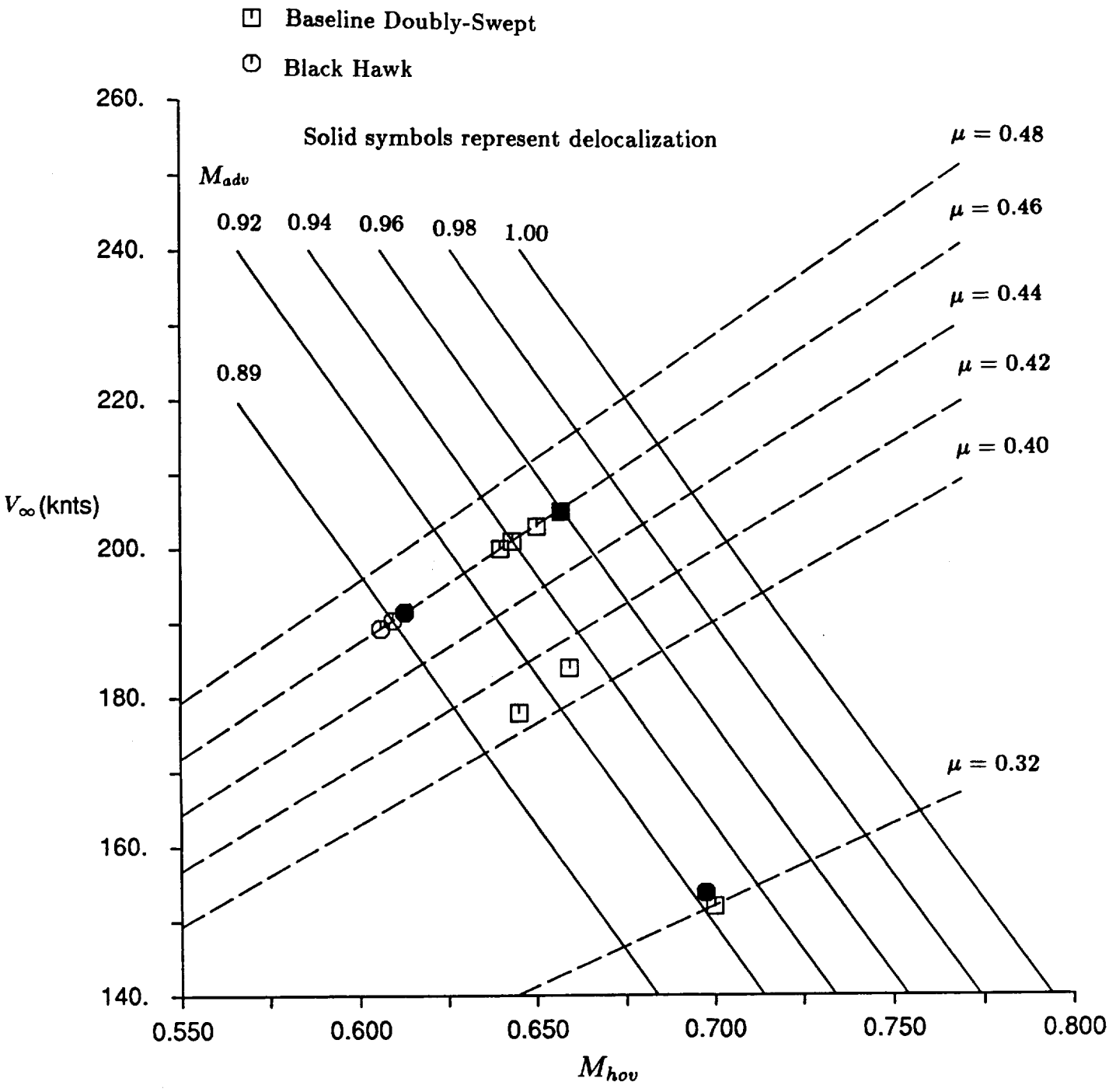

Figure 9. Nomograph for advancing tip Mach number and rotor advance ratio as a function of rotational tip Mach number and helicopter flight speed.

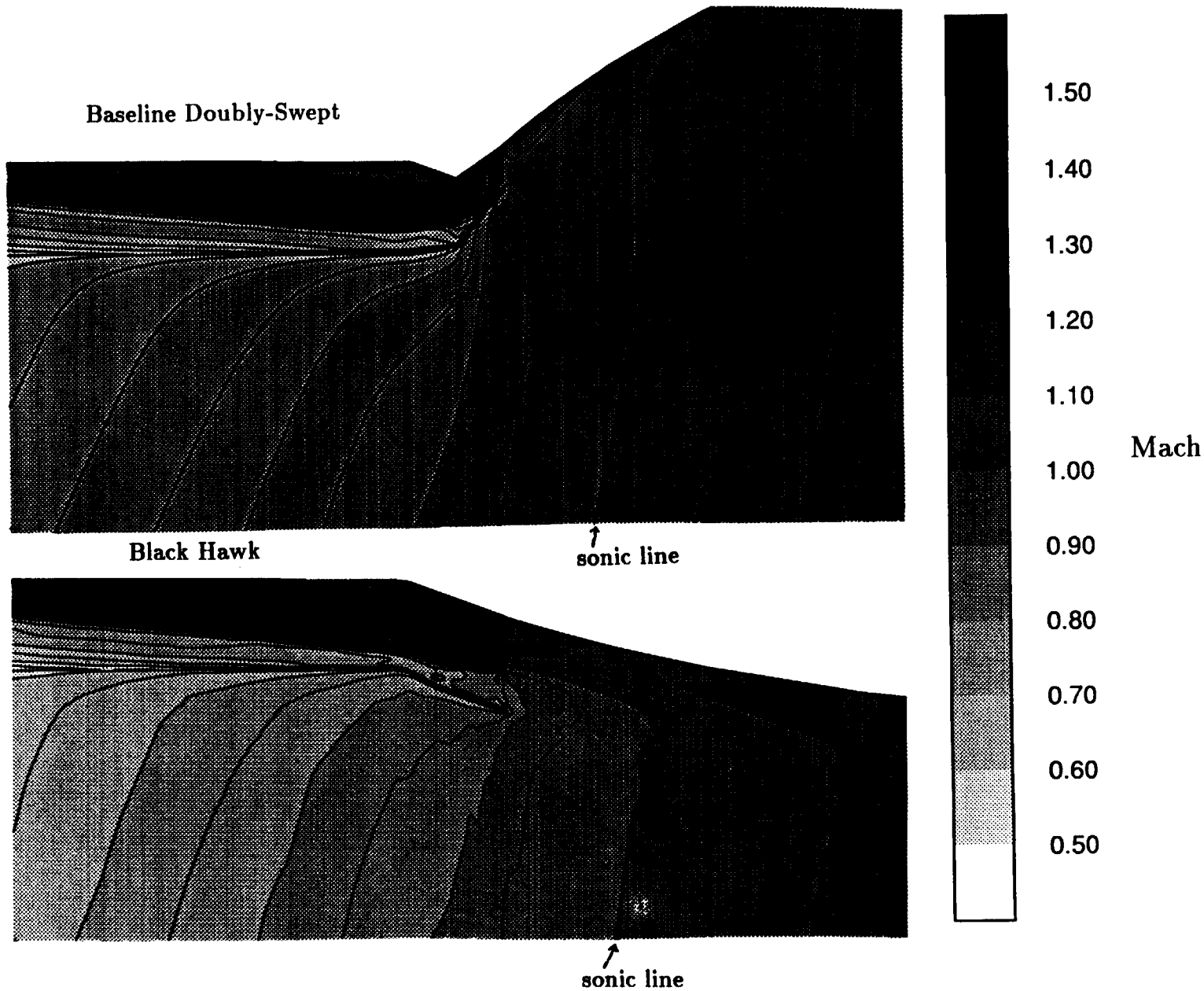

Figure 10. Mach contours for the baseline doubly-swept and Black Hawk blades at 90 degrees azimuth, $M_{adv} = 0.93$ ($\mu = 0.331$, $M_{hov} = 0.702$).

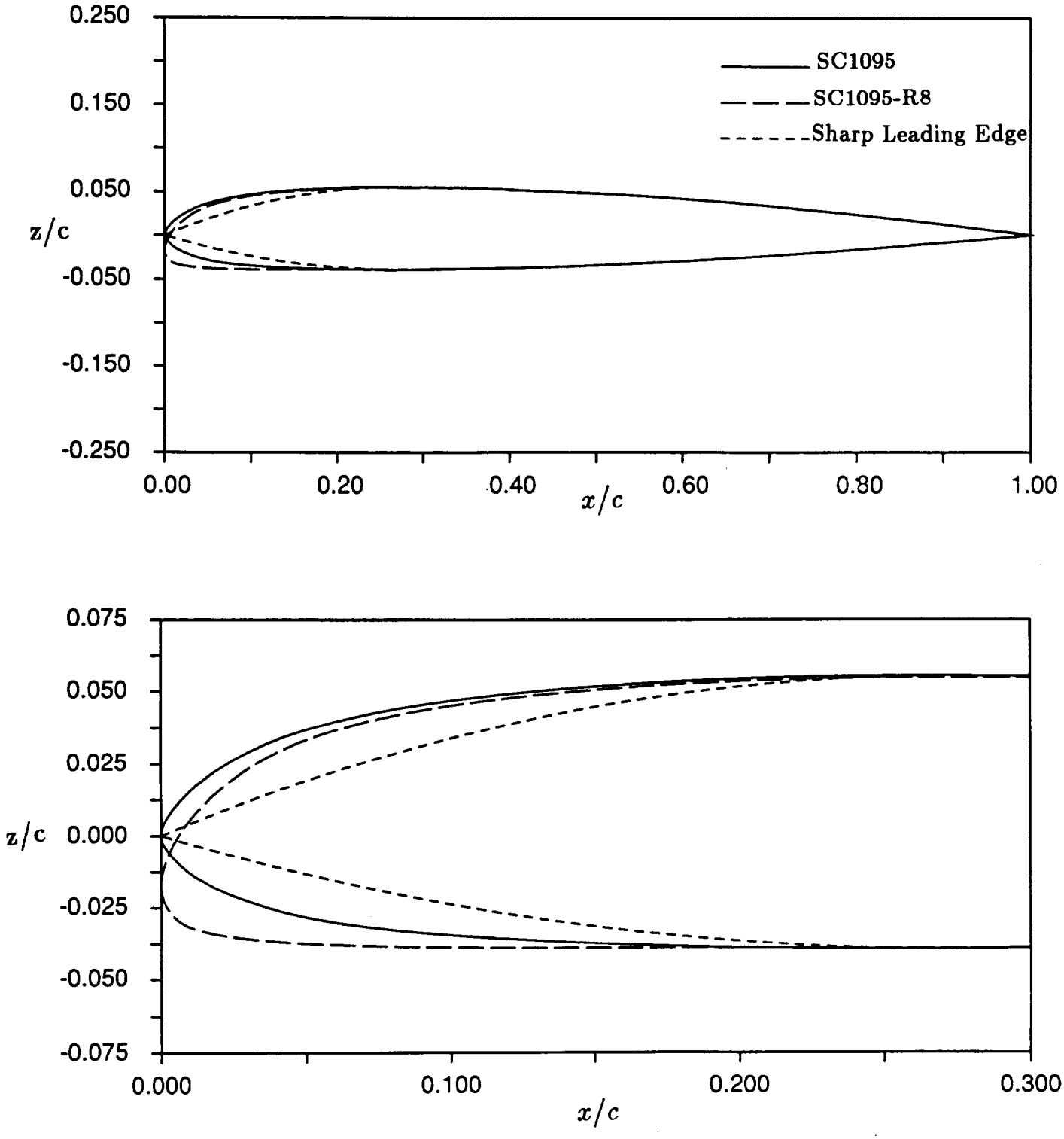

Figure 11. Airfoil cross-sections used for the blade designs: SC1095, SC1095-R8, sharp leading-edge airfoil used at the tip.

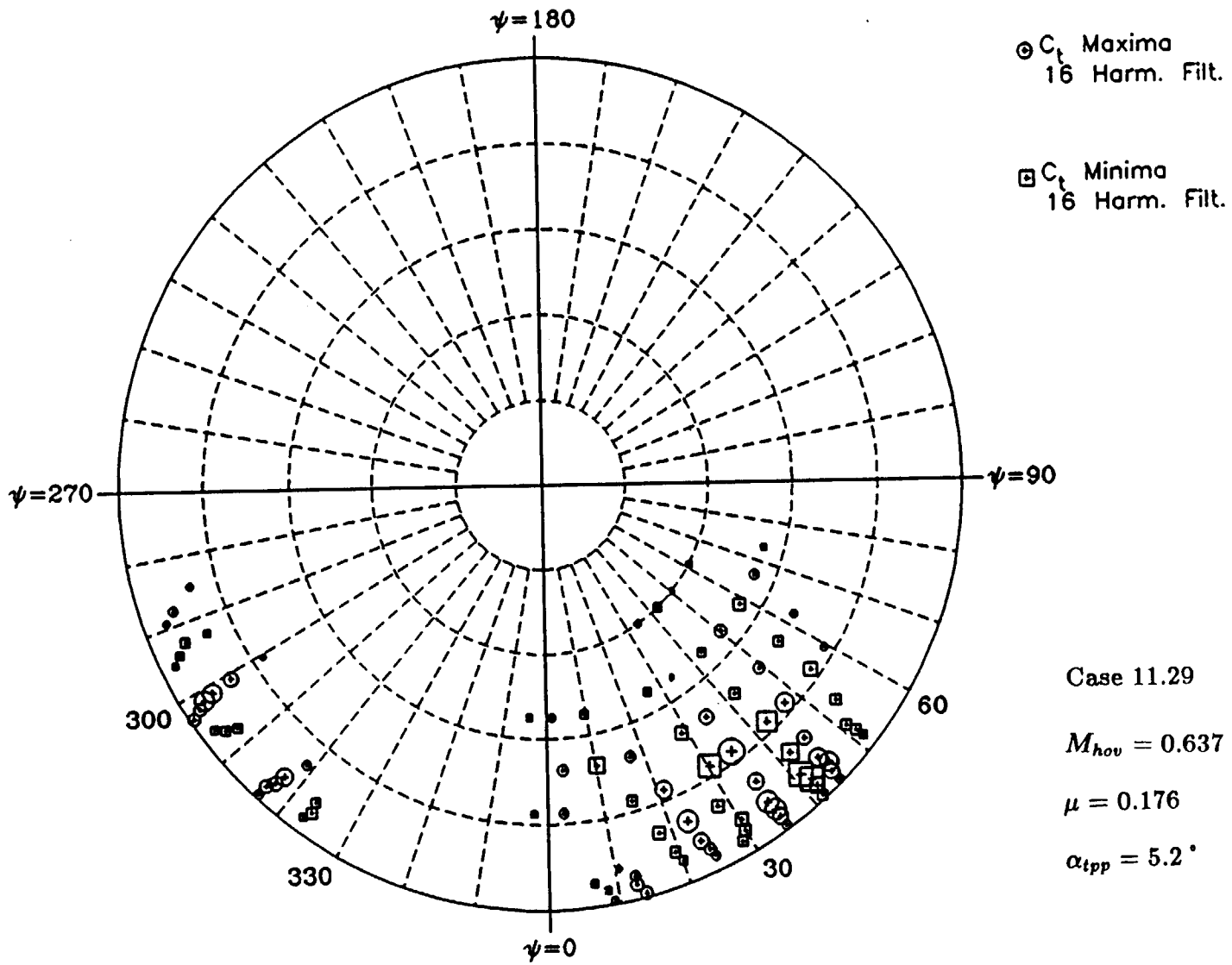

Figure 12. Peak loading locations conjectured to be related to BVI locations for the Black Hawk rotor.

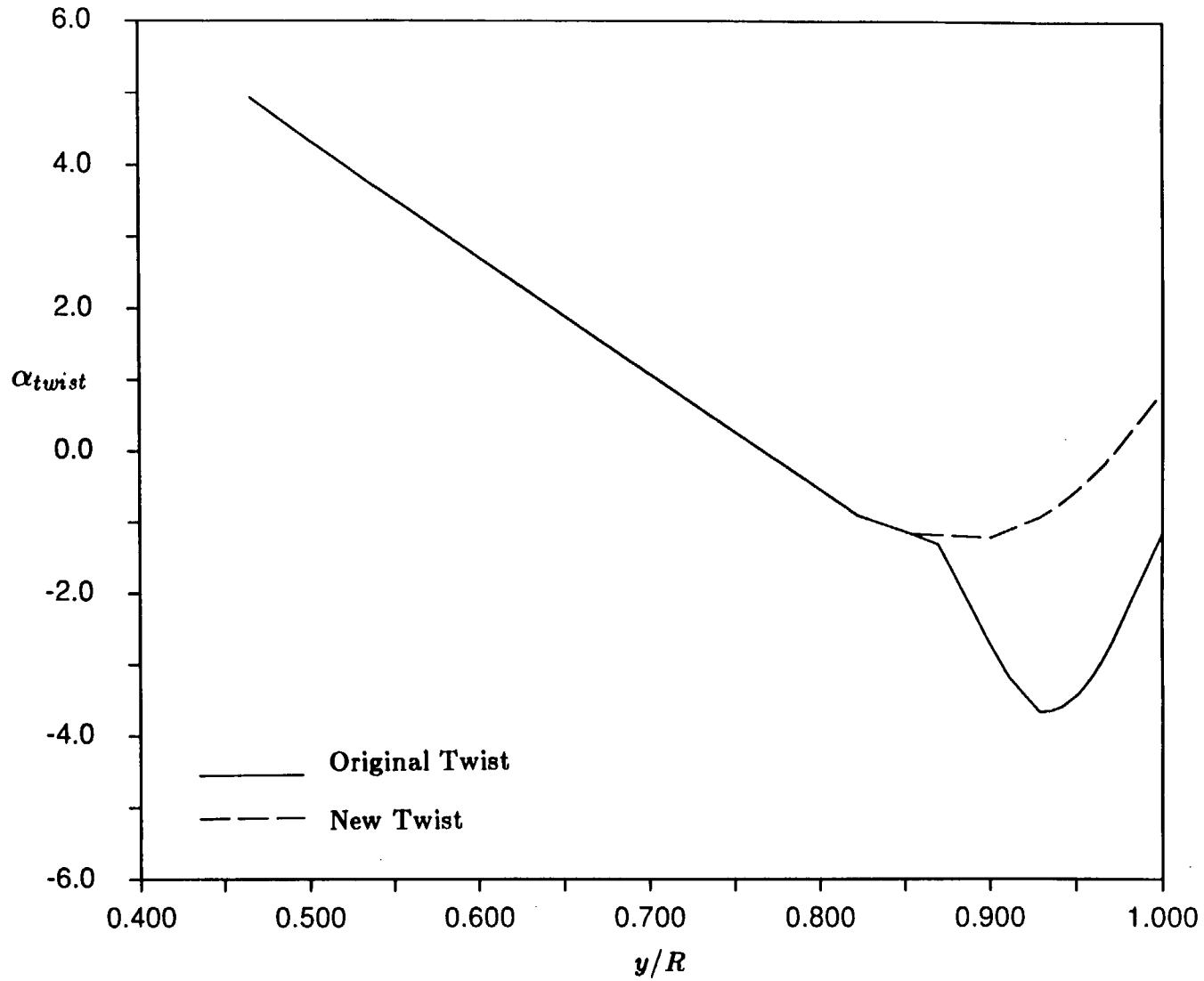

Figure 13. Modified twist distribution compared with the original twist.

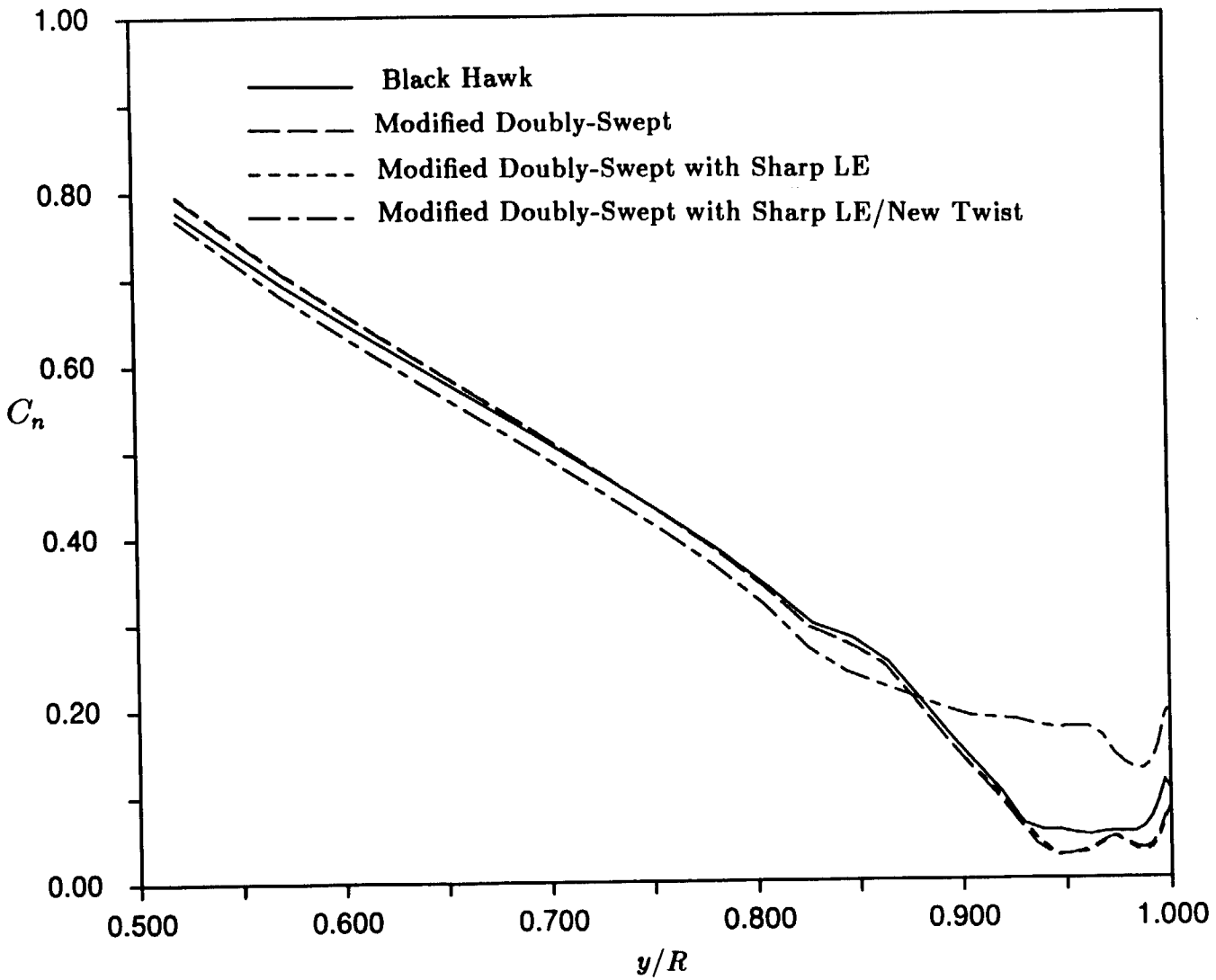

Figure 14. Normal force coefficient distributions of the four blade geometries at $\psi = 140\,^{\circ}$ for $\mu = 0.176$, $M_{hov} = 0.637$.

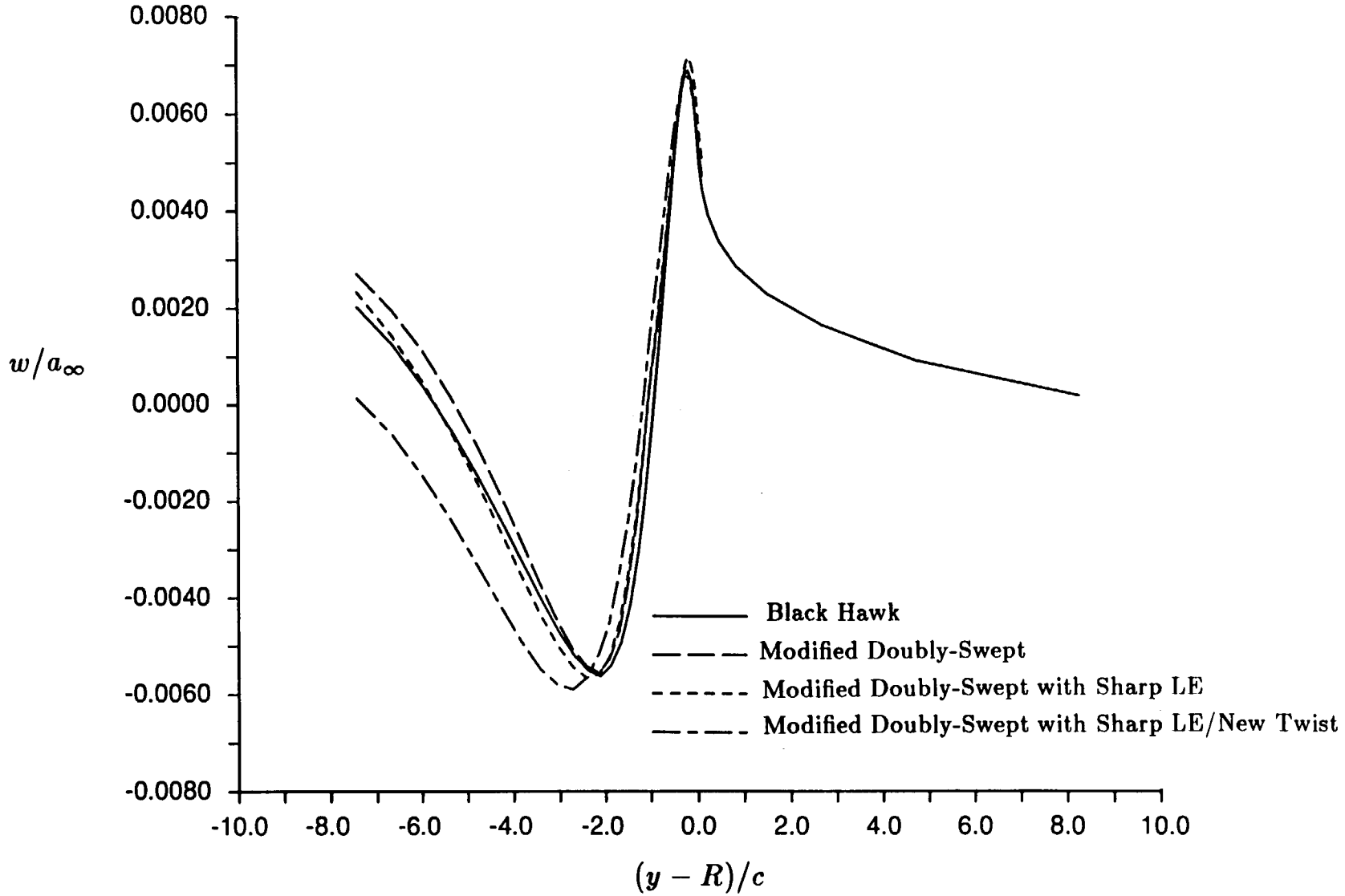

Figure 15. Axial velocity profiles for the four blades at six chords downstream.

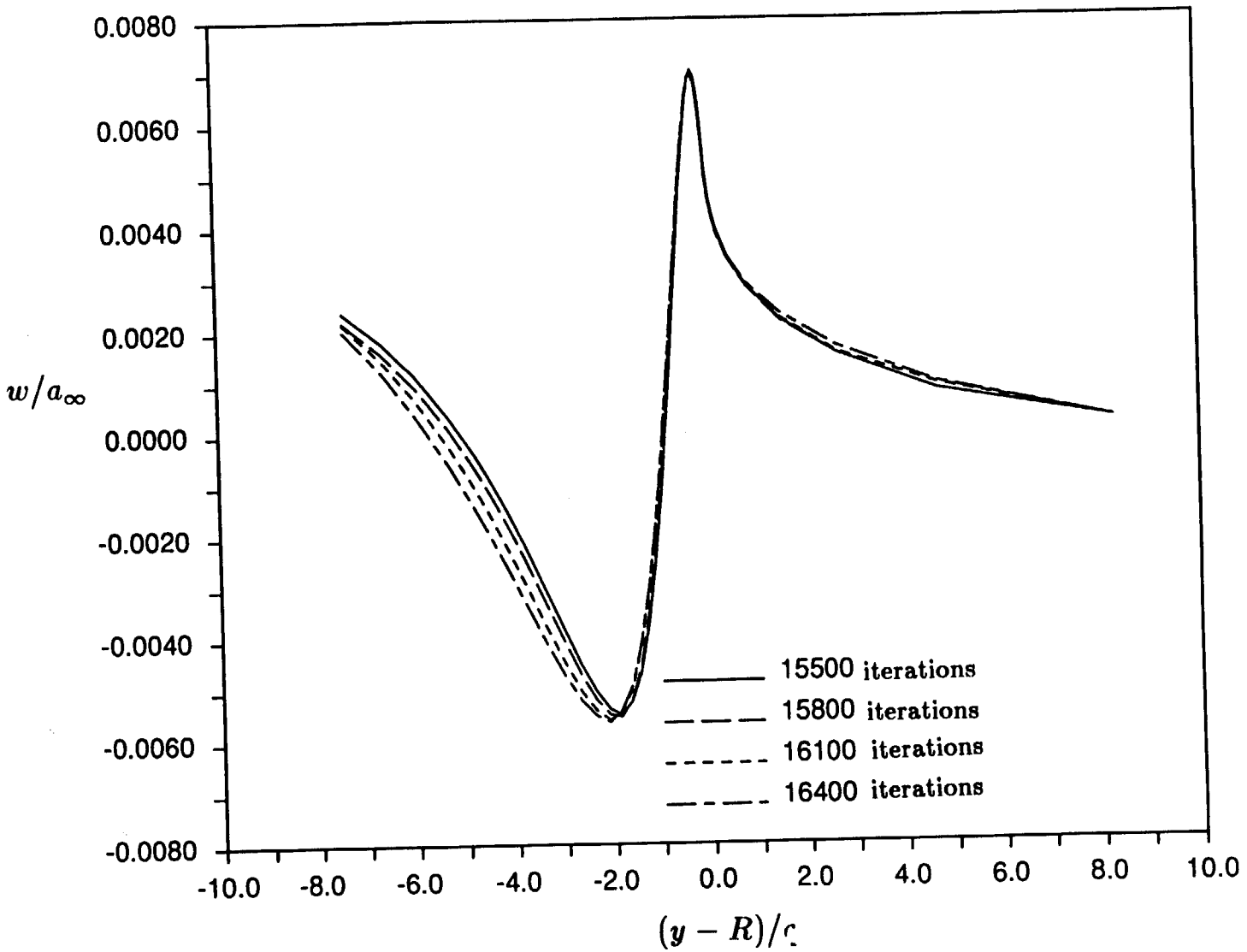

Figure 16. Convergence of axial velocity distribution at six chords downstream.

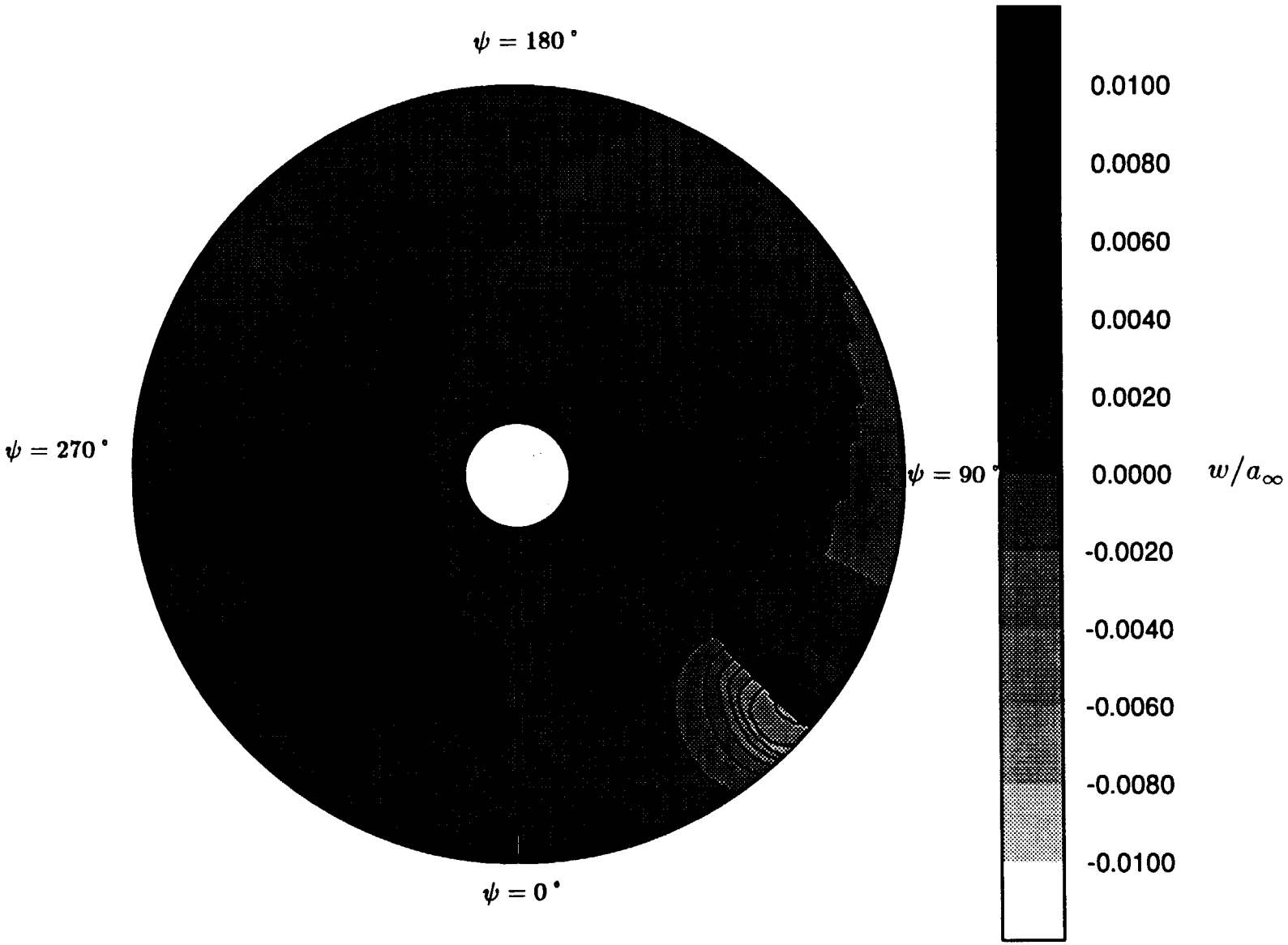

Figure 17a. Inflow distribution over the rotor disc for the Black Hawk blade.

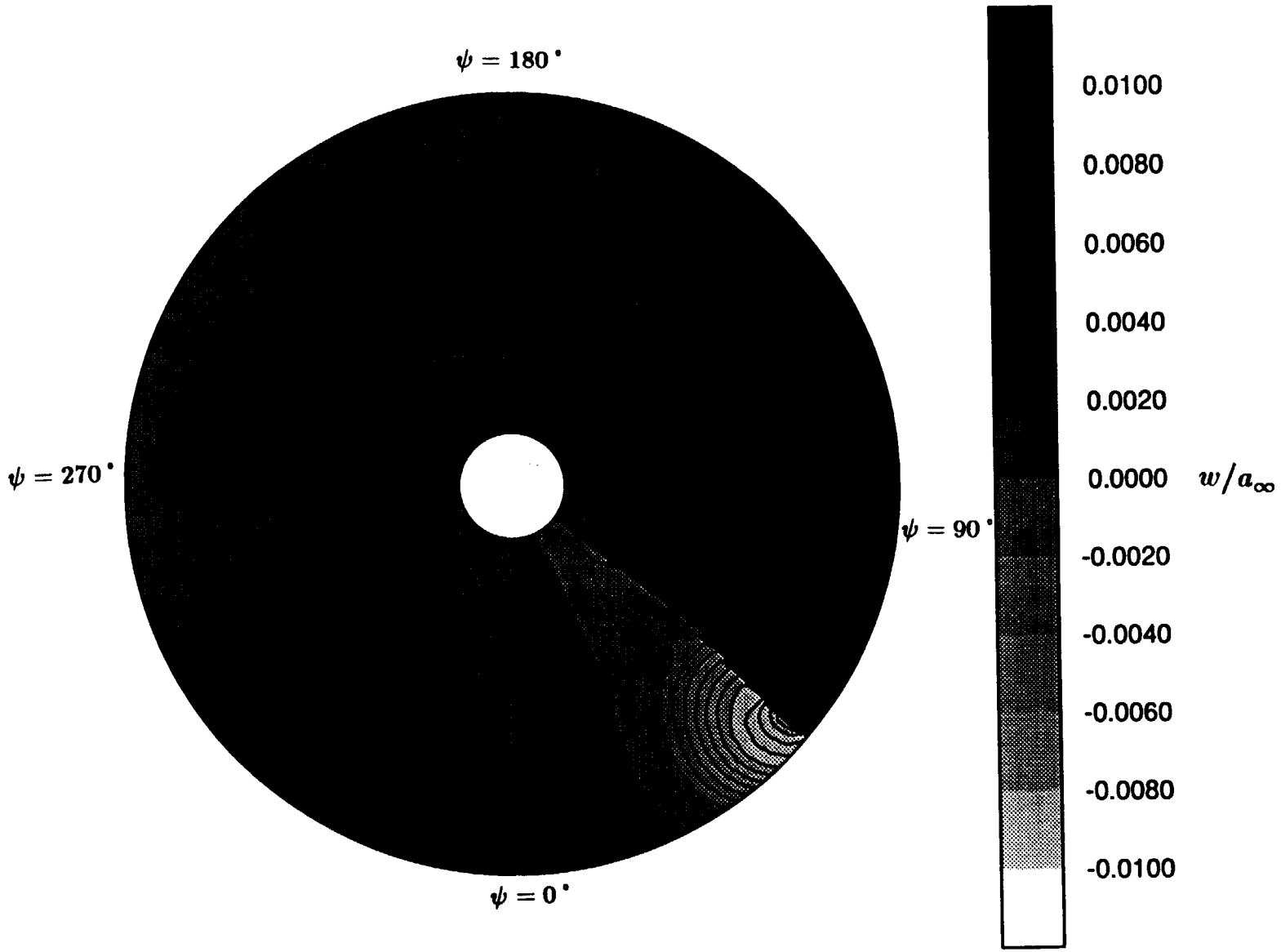

Figure 17b. Inflow distribution over the rotor disc for the baseline doubly-swept blade.

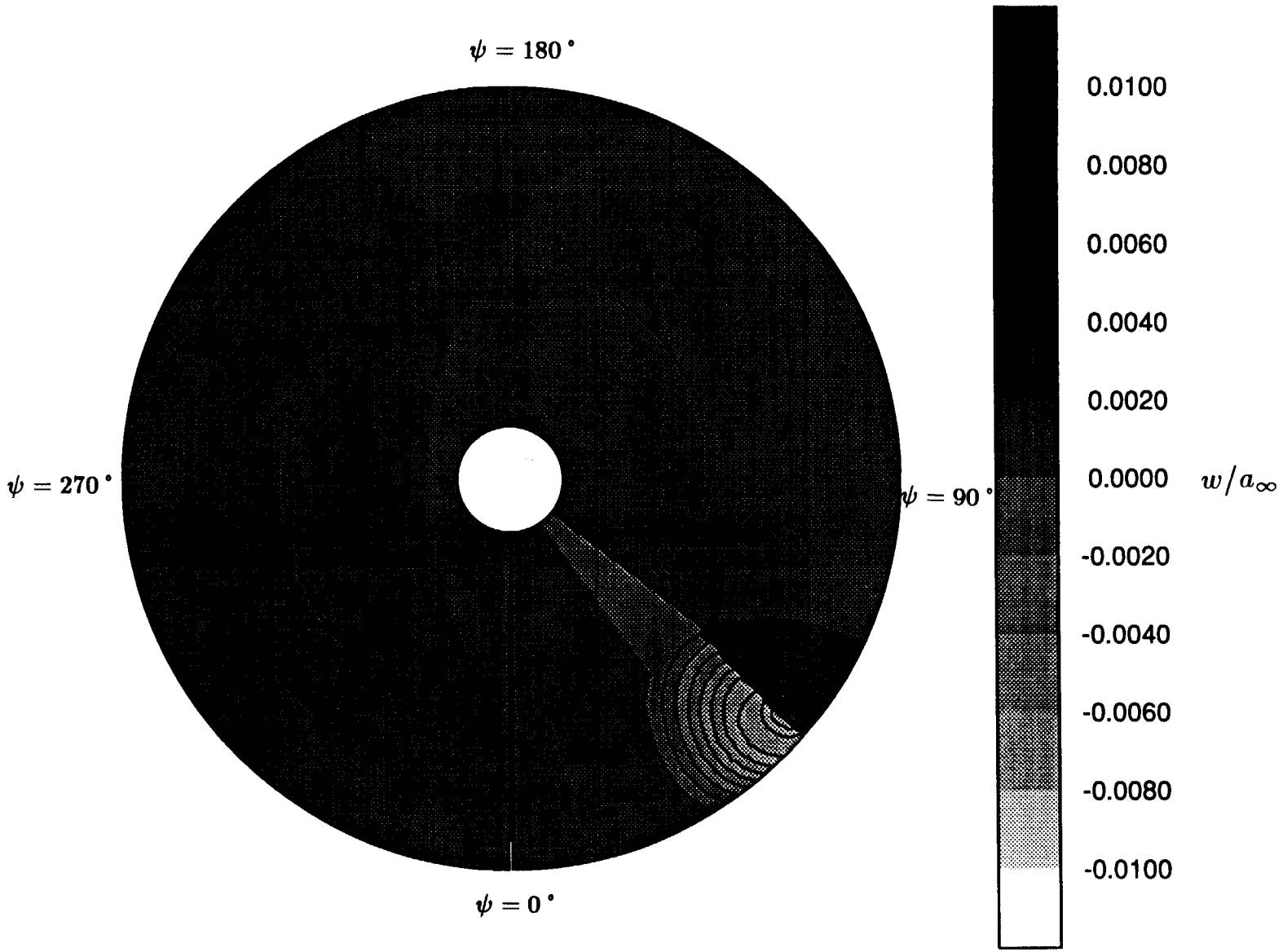

Figure 17c. Inflow distribution over the rotor disc for the modified doubly-swept blade with sharp-leading edge/new twist.

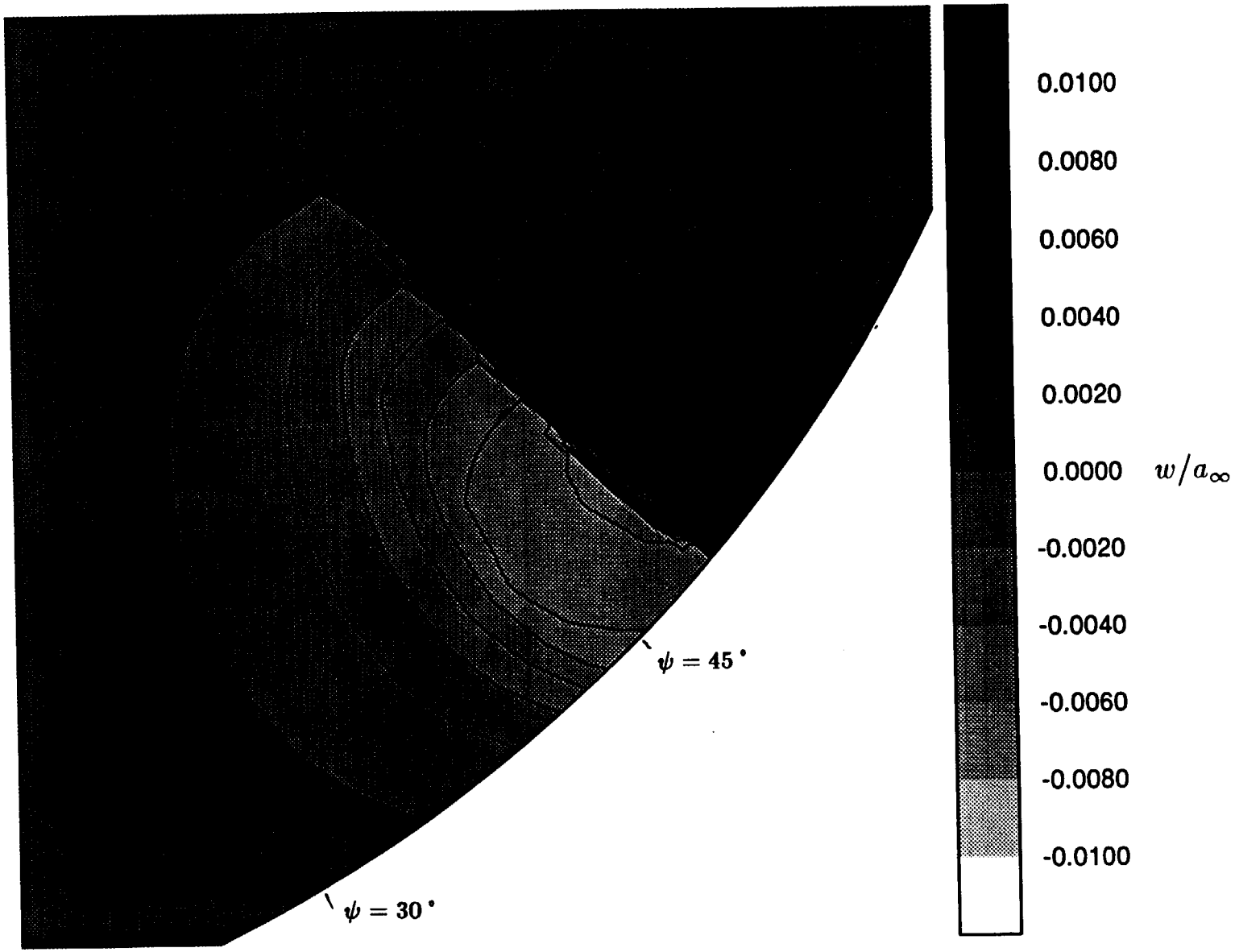

Figure 18a. Inflow distribution near the BVI event for the Black Hawk blade.

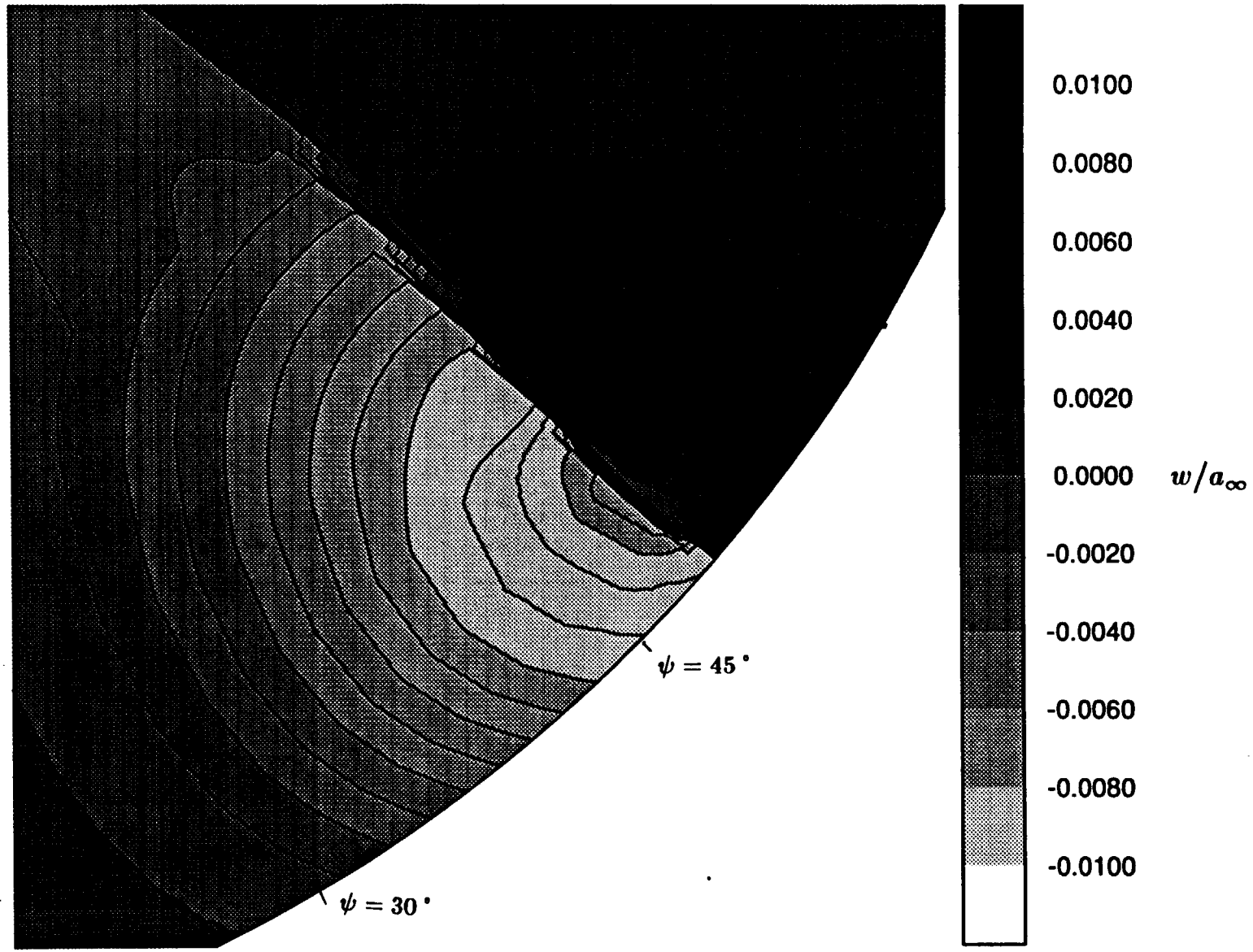

Figure 18b. Inflow distribution near the BVI event for the baseline doubly-swept blade.

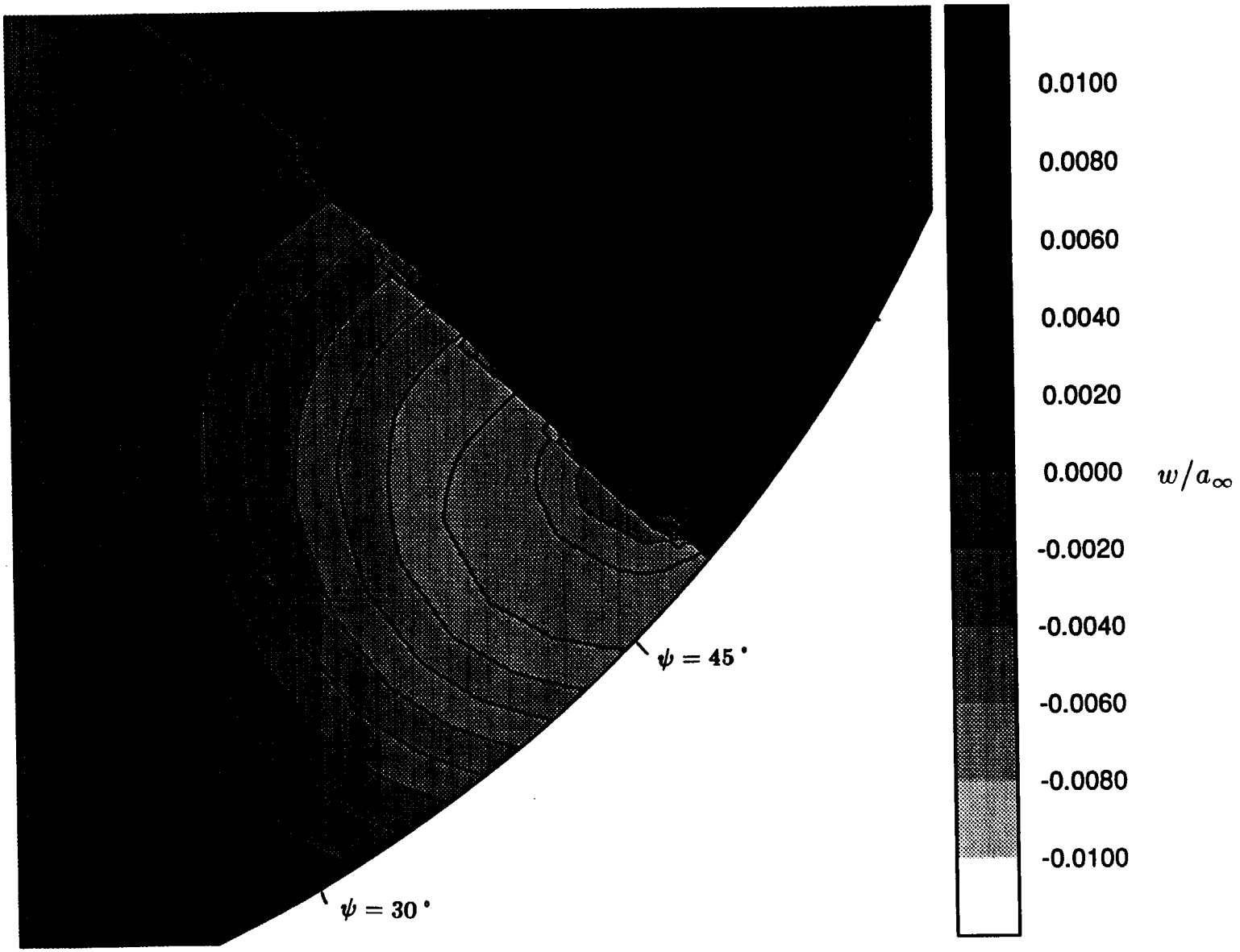

Figure 18c. Inflow distribution near the BVI event for the modified doubly-swept blade with sharp-leading edge/new twist.

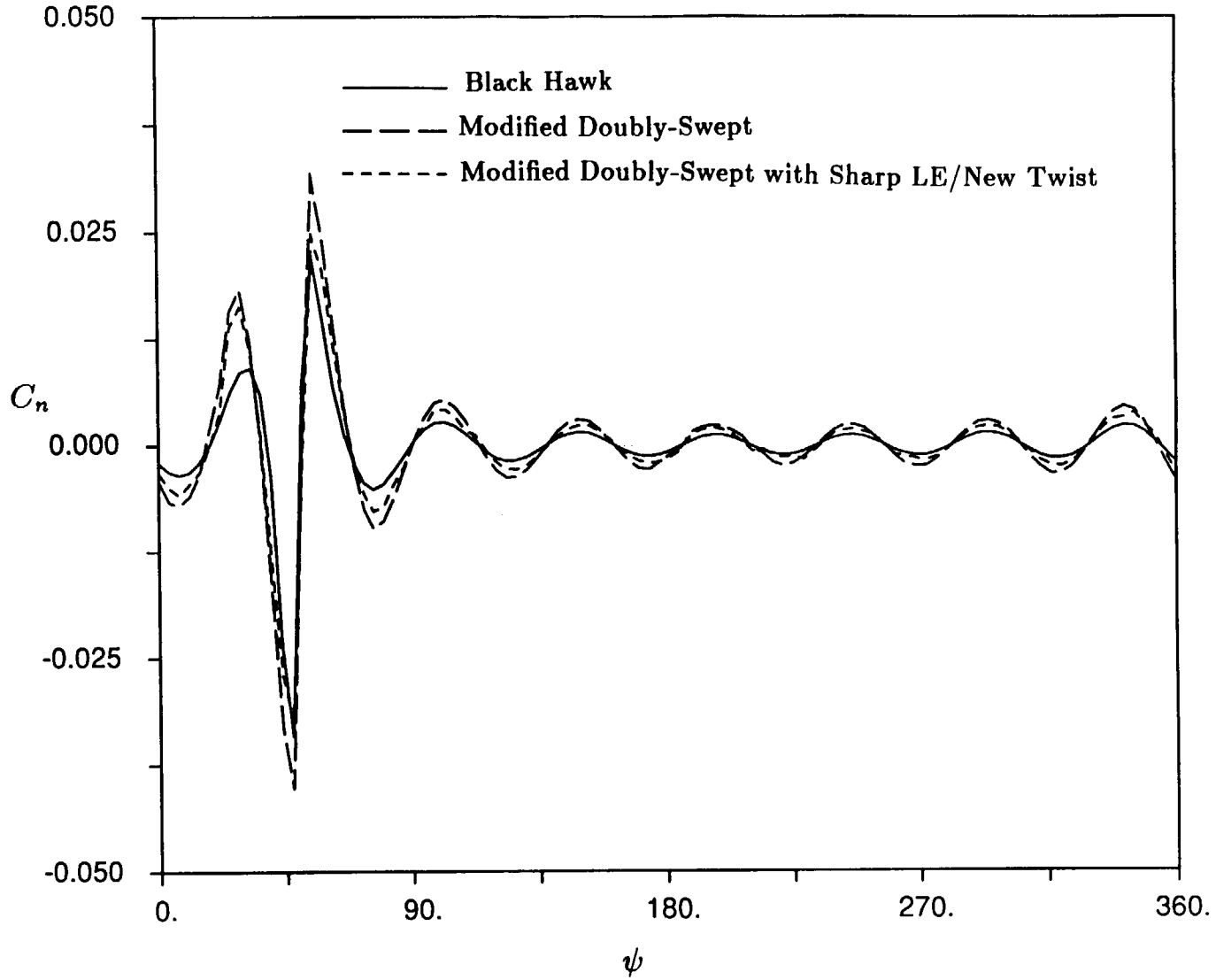

Figure 19. Higher-harmonic content of sectional normal force coefficient time histories for the BVI event (harmonics $\geq$ two blade-passage frequencies).

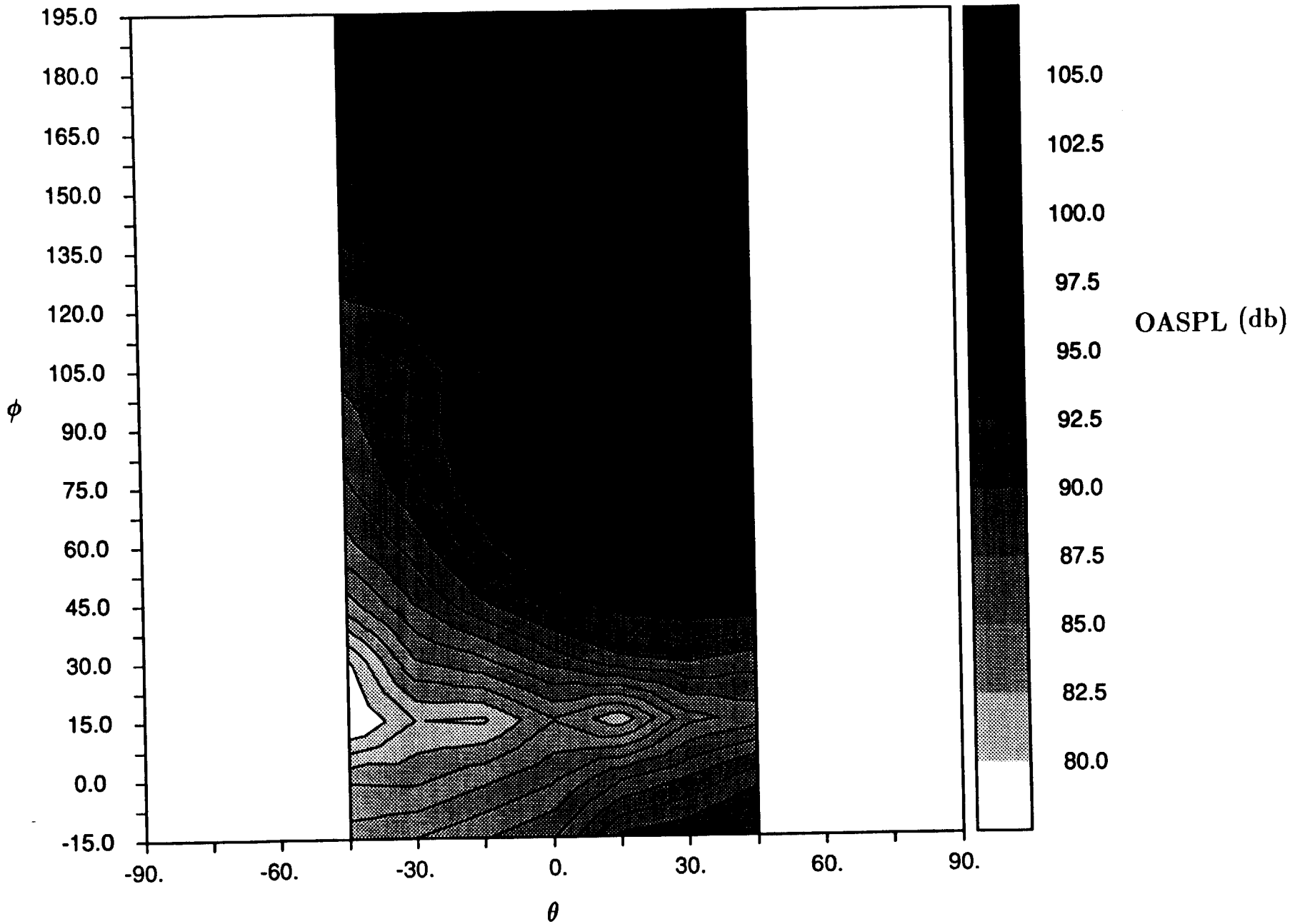

Figure 20a. Contours of overall sound pressure level (OASPL) below the rotor with Black Hawk blades.

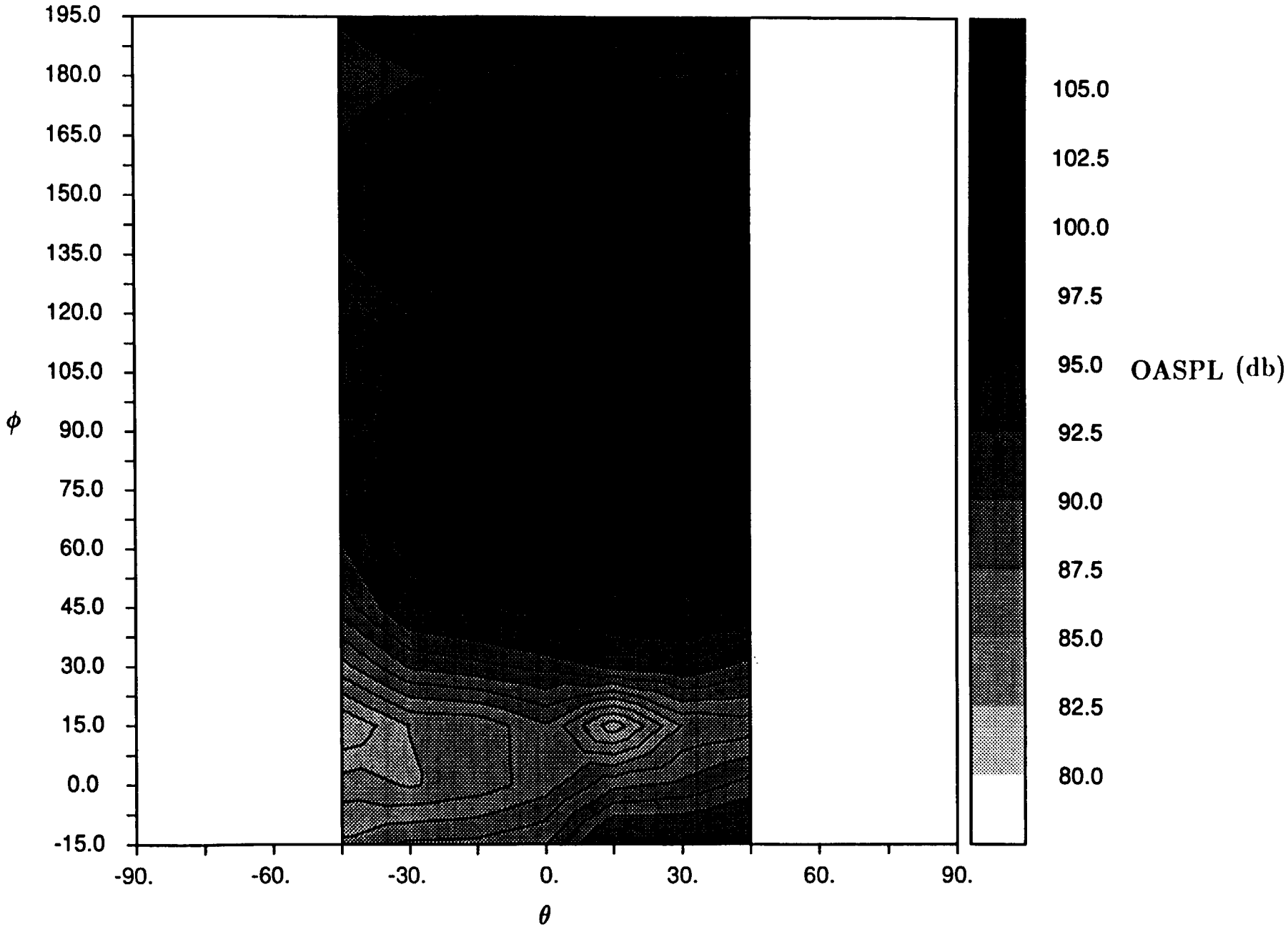

Figure 20b. Contours of overall sound pressure level (OASPL) below the rotor with baseline doubly-swept blades.

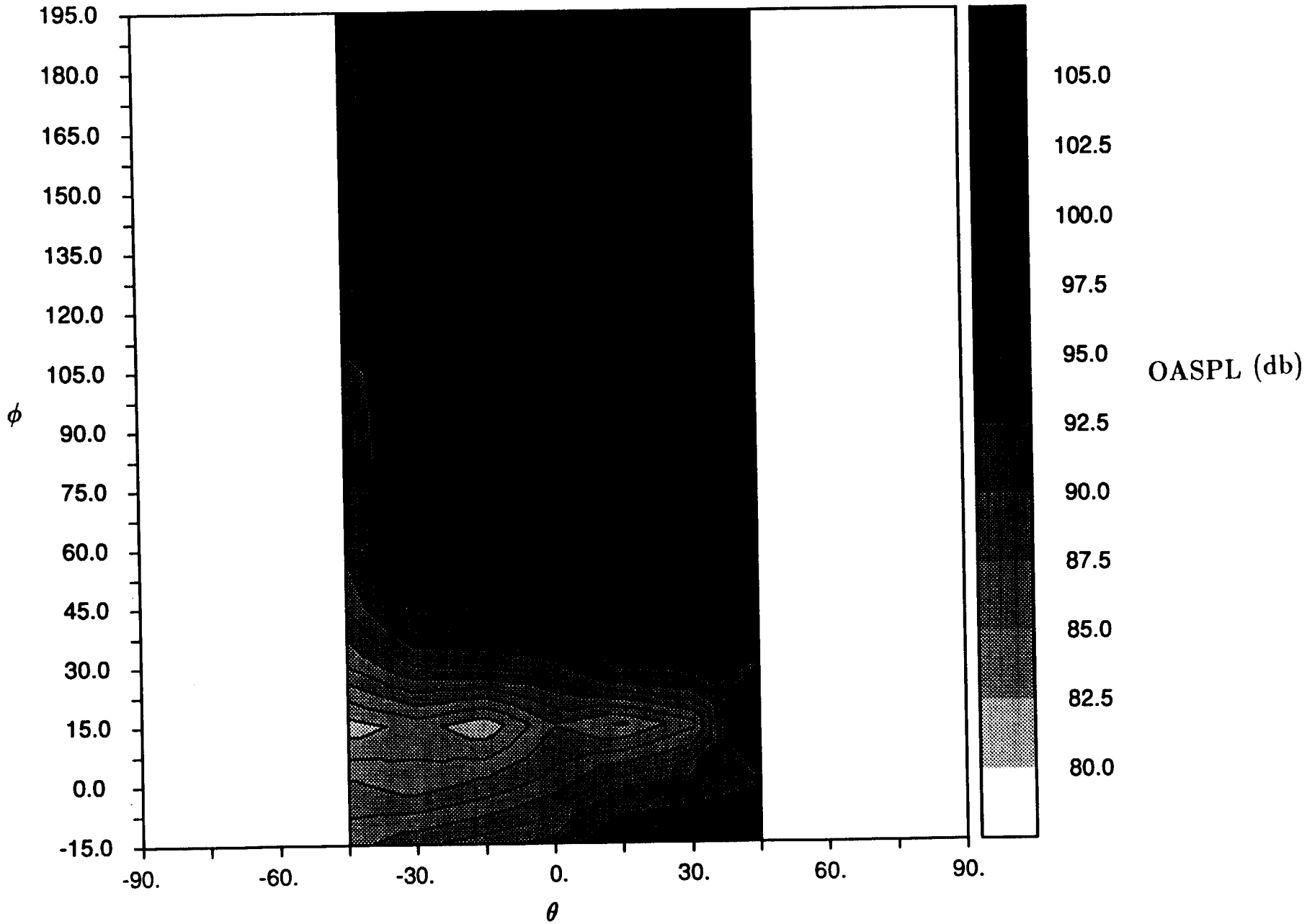

Figure 20c. Contours of overall sound pressure level (OASPL) below the rotor modified doubly-swept blades with sharp leading edge/new twist.

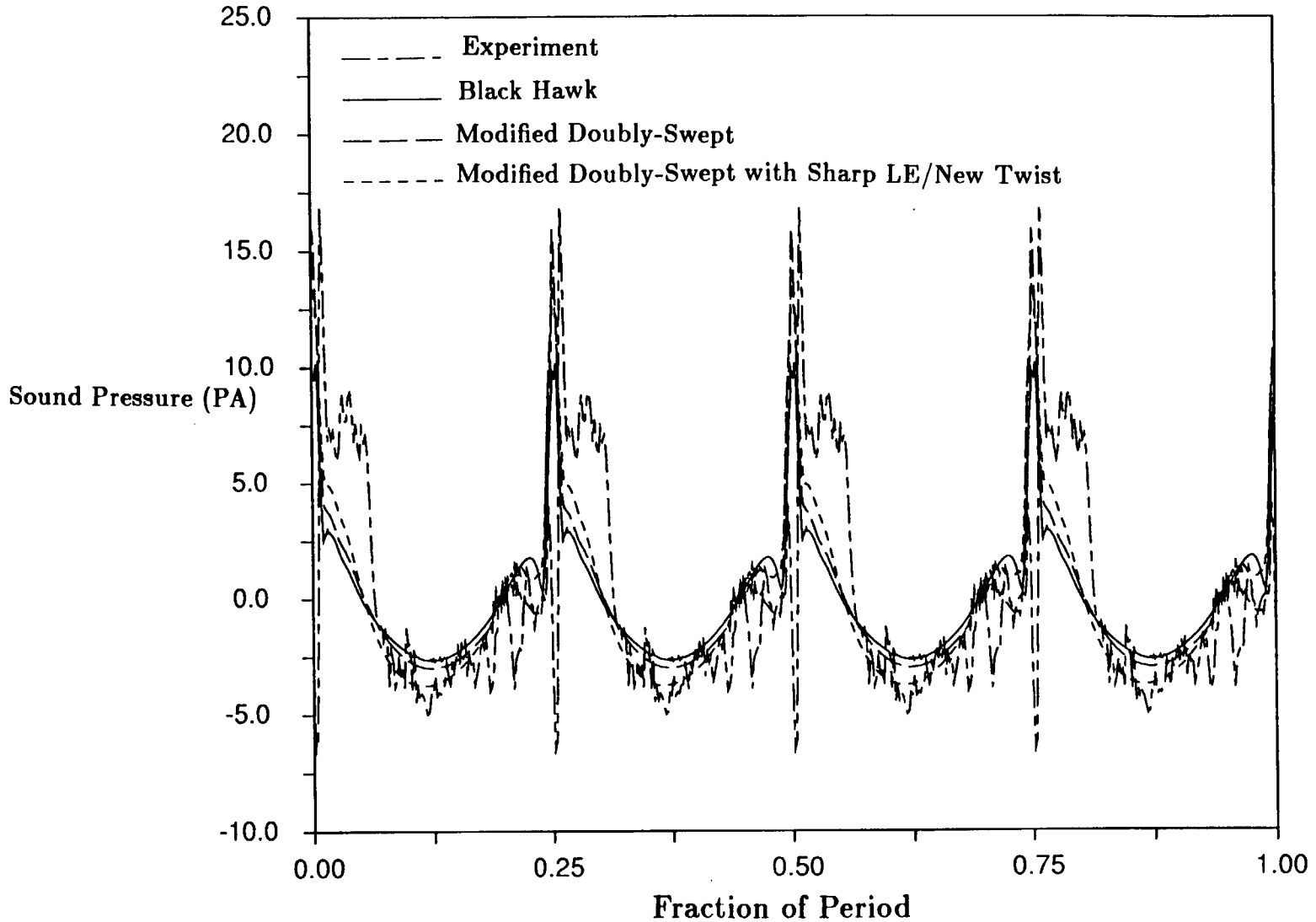

Figure 21. Acoustic pressure signal for BVI event for the three blade geometries and experiment at $\theta = 30$ deg. and $\phi = 150$ deg.

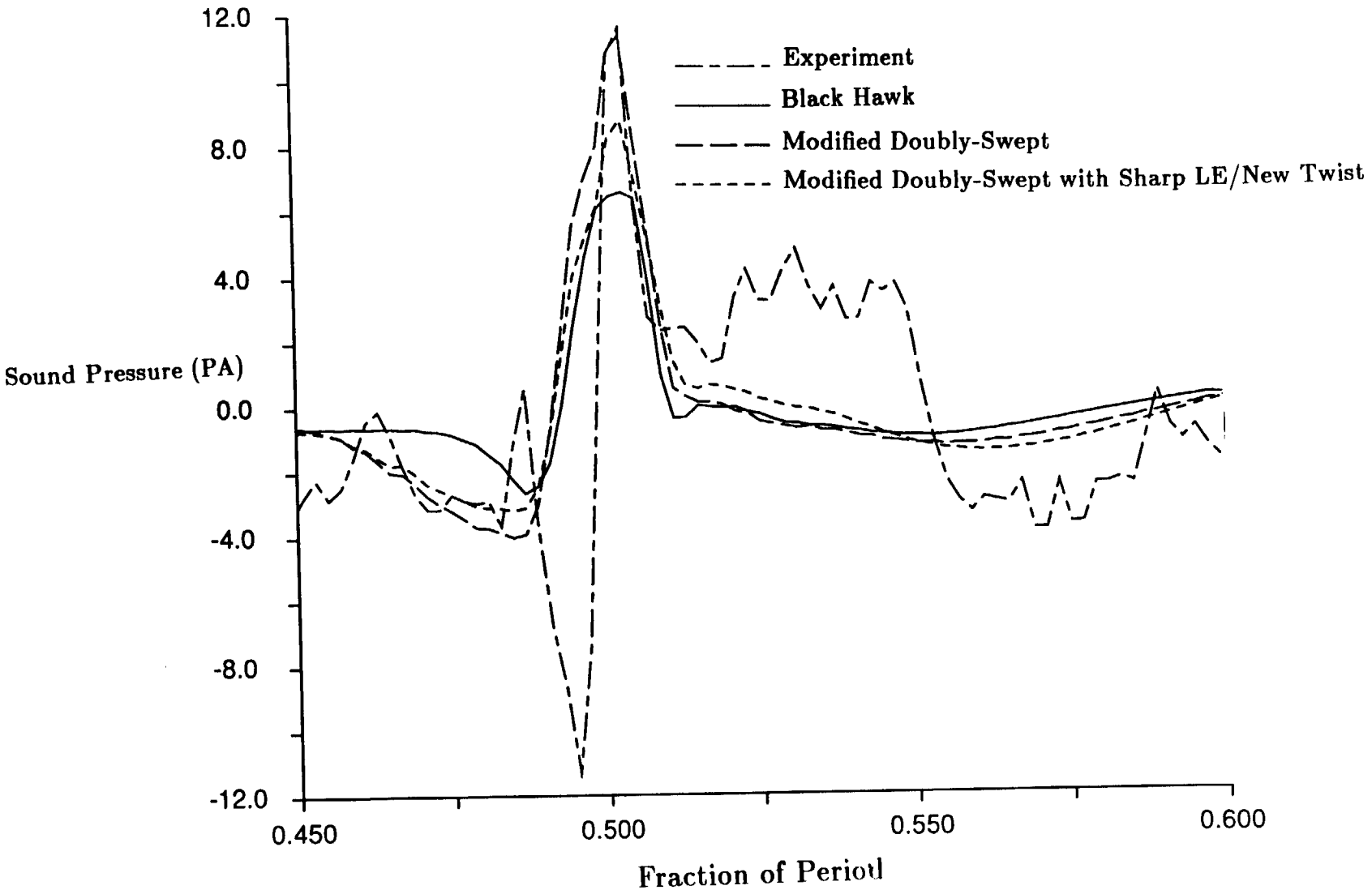

Figure 22. Acoustic pressure signal for BVI event for the three blade geometries and experiment at $\theta = 30$ deg. and $\phi = 150$ deg (harmonics $\geq$ two blade-passage frequencies).

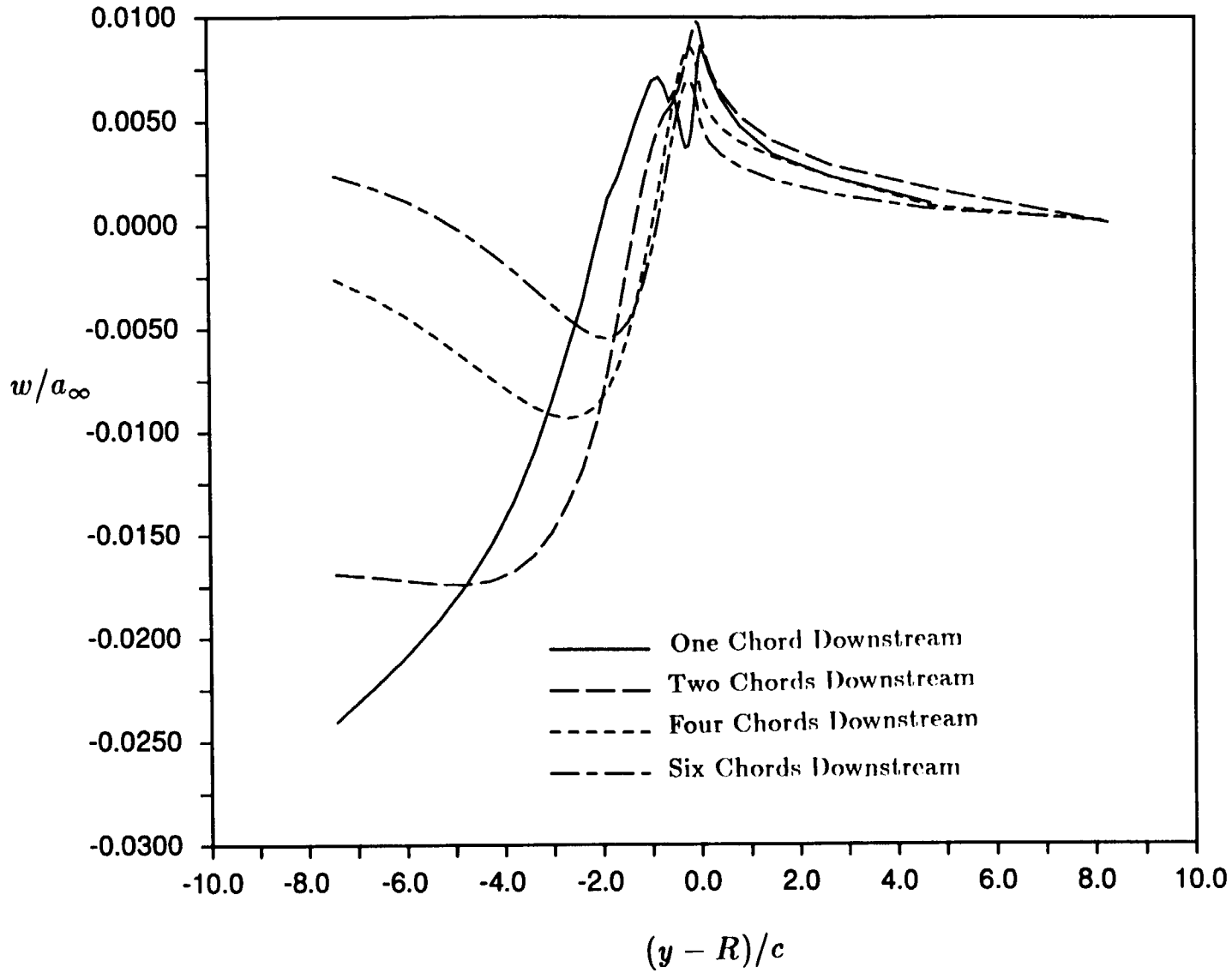

Figure 23. Axial velocity profiles for the Black Hawk blade at several locations downstream.

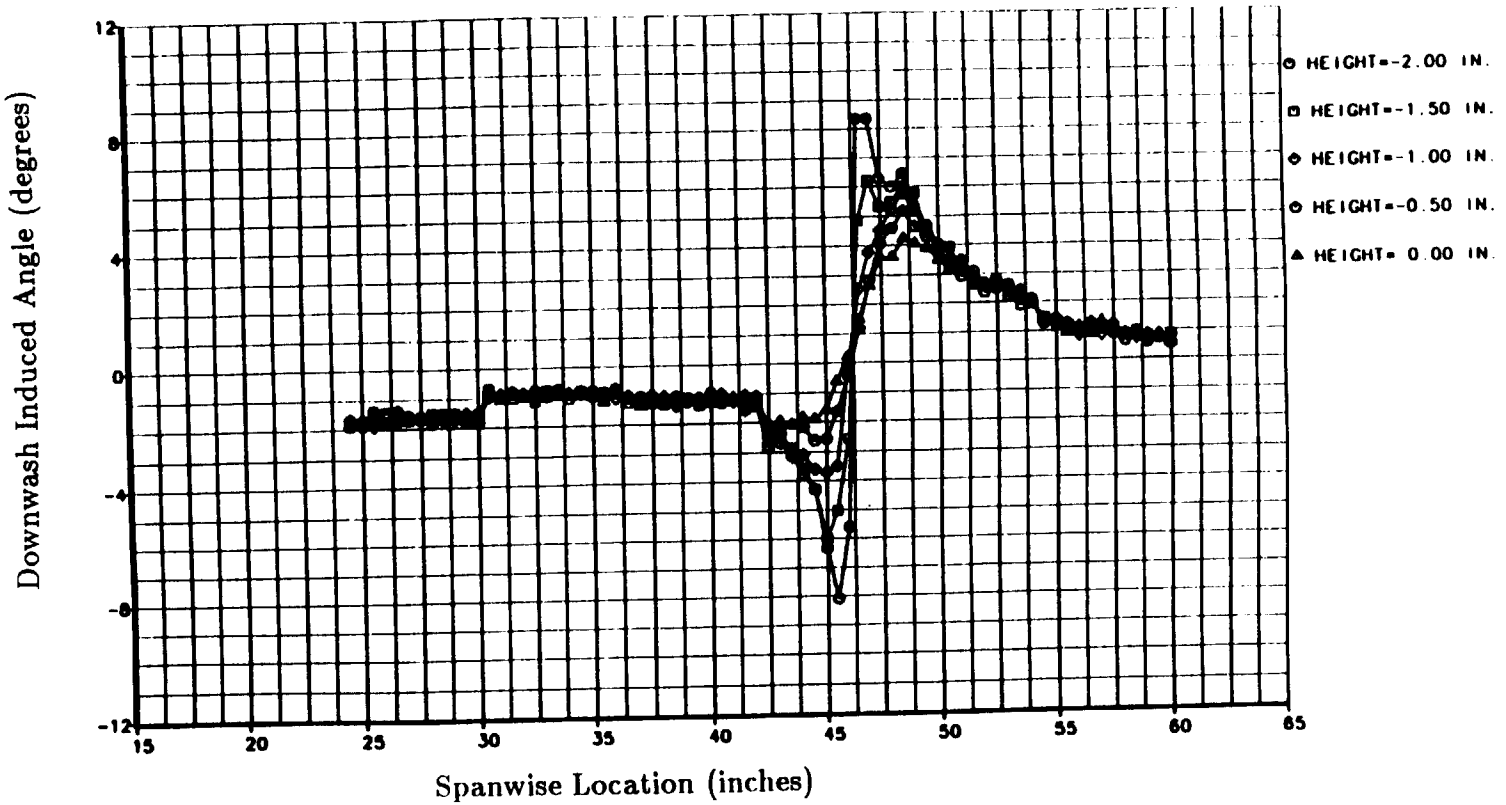

Figure 24. Experimental values of induced downwash angles for the tip vortex of the blade from Ref. 61.

REPORT DOCUMENTATION PAGE

Form Approved
OMB No. 0704-0188

1. AGENCY USE ONLY (Leave blank)	2. REPORT DATE	3. REPORT TYPE AND DATES COVERED

4. TITLE AND SUBTITLE
Evaluation of a Doubly-Swept Tip for Rotorcraft Noise Reduction

5. FUNDING NUMBERS
C NAS1-19143

6. AUTHOR(S)
Brian E. Wake
T. Alan Egolf

7. PERFORMING ORGANIZATION NAME(S) AND ADDRESS(ES)
United Technologies Research Center
400 Main Street
MS 129-18
East Hartford, CT 06108

8. PERFORMING ORGANIZATION REPORT NUMBER

9. SPONSORING/MONITORING AGENCY NAME(S) AND ADDRESS(ES)
NASA
Langley Research Center
Hampton, VA 23681-0001

10. SPONSORING/MONITORING AGENCY REPORT NUMBER
NASA CR-189677

11. SUPPLEMENTARY NOTES
Langley Technical Monitor: Earl R. Booth, Jr.

12a. DISTRIBUTION/AVAILABILITY STATEMENT
[redacted]
Subject Category 71

12b. DISTRIBUTION CODE

13. ABSTRACT *(Maximum 200 words)*

A computational study was performed for a doubly-swept rotor blade tip to determine its benefit for high-speed impulsive (HSI) and blade-vortex interaction (BVI) noise. This design consists of aft and forward sweep. For the HSI-noise computations, unsteady Euler calculations were performed for several variations to a rotor blade geometry. A doubly-swept planform was predicted to increase the delocalizing Mach number to 0.94 (representative of a 200+ kt helicopter). For the BVI-noise problem, it had been hypothesized that the doubly-swept blade tip, by producing a leading-edge vortex, would reduce the tip-vortex effect on BVI noise. A procedure was used in which the tip-vortex velocity profile computed by a Navier-Stokes solver was used to compute the inflow associated with BVI. This inflow was used by an Euler solver to compute the unsteady pressures for an acoustic analysis. The results of this study were inconclusive due to the difficulty in accurately predicting the viscous tip vortex downstream of the blade. Also, for the condition studied, no leading-edge vortex formed at the tip.

14. SUBJECT TERMS
Navier-Stokes Rotorcraft
Acoustics Euler

15. NUMBER OF PAGES
68

16. PRICE CODE

17. SECURITY CLASSIFICATION OF REPORT	18. SECURITY CLASSIFICATION OF THIS PAGE	19. SECURITY CLASSIFICATION OF ABSTRACT	20. LIMITATION OF ABSTRACT
Unclassified	Unclassified	Unclassified	